AN INVESTIGATION OF THE PRODUCTION OF MAGNUS FORCES ON A HIGH FINENESS RATION BODY OF REVOLUTION

Timothy Robert Beard

NAVAL POSTGRADUATE SCHOOL
Monterey, California

THESIS

AN INVESTIGATION OF THE PRODUCTION OF
MAGNUS FORCES ON A
HIGH FINENESS RATIO BODY OF REVOLUTION

by

Timothy Robert Beard

Thesis Advisor: Howard L. Power Jr.

March 1973

An Investigation of the Production of Magnus Forces on a High Fineness Ratio Body of Revolution

by

Timothy Robert Beard
Lieutenant, United States Navy
B.S., United States Naval Academy, 1966

Submitted in partial fulfillment of the
requirements for the degree of

MASTER OF SCIENCE IN AERONAUTICAL ENGINEERING

from the

ABSTRACT

A high fineness ratio body of revolution with an ogive forebody shape was tested at varying angles of attack, Reynolds numbers, and spin rates to measure the Magnus forces developed. The experimental data were compared with previously derived theoretical equations for an open-ended cylinder of revolution to substantiate the theoretical work.

TABLE OF CONTENTS

ACKNOWLEDGEMENT

The author wishes to express his sincere appreciation to his advisor, Asst. Professor Howard L. Power, for his guidance and help in preparing this thesis, and to Mr. Glenn A. Middleton and Mr. Cecil R. Gordon of the Naval Postgraduate School Aeronautics Department staff for their help in constructing the model and electronic equipment.

I would also like to thank my wife, Melissa, for her patience during my work.

NOMENCLATURE

C_Y - side force coefficient based on frontal area

D - diameter of missile

L - length of missile

$\bar{p}$ - dimensionless spin rate

q - freestream dynamic pressure

R_L - Reynolds number based on missile length

R_C - cross flow Reynolds number based on missile diameter

S - missile maximum cross sectional area

T - air temperature

U - freestream velocity

Y - Magnus side force

α - angle of attack

Γ - circulation

μ - coefficient of viscosity

ρ - air density

ω - spin angular velocity

INTRODUCTION

The study of flight trajectories of spin stabilized missiles requires detailed analyses of the aerodynamic forces developed during flight. The projectile's lift, drag, and side force must be accurately predicted for studies of this kind. This paper investigates the flow over a high fineness ratio spinning body of revolution to determine the side force and its center of pressure generated during flight. The side force causes drift from the plane of firing and so is an important aerodynamic force.

Determining the flow over a missile is a very complicated three-dimensional problem in which the primary mechanism for production of the side force is shed vorticity caused by the eventual separation of the boundary layer. Because of this the flow problem is dominated by viscous effects. Several theories have been developed to date to predict the side force and moment on open-ended cylinders, assuming laminar boundary layers. These theories, however, have yet to be substantiated experimentally in their appropriate regions of validity. For this reason a suitable testing apparatus and test program were devised to substantiate these theories. This thesis presents work accomplished to date on such studies.

HISTORICAL BACKGROUND

The study of spinning shapes and the side forces developed by them has been carried on for many years. To properly understand the complicated flow over a high fineness ratio body of revolution it is useful to study past investigations made on less complex spinning bodies.

In 1671 G. T. Walker [1] recorded the first description of drift of a spinning body in flight, the curve of a sliced tennis ball. Nearly 200 years later G. Magnus [2] published the results of his experiments to account for the drift of a spinning musket shot. Magnus' method was to fire a musket ball whose center of mass was not at its geometric center and thus impose a spin on the ball as it left the gun barrel. Magnus found a clockwise rotation would cause the ball to drift right and a counter-clockwise rotation would cause a drift to the left. This substantiated his theory that an aerodynamic force was responsible for the drift. Any such side force produced by a spinning body is today called a Magnus force.

Lord Rayleigh published a paper in 1877 entitled "On the Irregular Flight of a Tennis Ball" [3] in which he mathematically described the Magnus effects in terms of a potential flow around a cylinder with circulation. Missing from his theory, however, were skin friction effects

between the fluid and cylinder which related the cylinder spinning rate to the magnitude of the assumed circulation.

Little or no theory followed Rayleigh's work until after World War I. Shortly after the war a notable attempt was made to use the Magnus effect commercially by a German named Anton Flettner [4]. He replaced the sails of a ship with a large powered rotor. In a cross-wind the Magnus effect would power the ship. Two Flettner Rotor Ships were built and one sailed across the Atlantic, but the speed and reliability of screw propulsion proved to be the rotor ship's downfall.

In 1924 Prandtl [5] published his work on the problem of creation of circulation about a spinning body. He was able to show that circulation was developed and could be accounted for by shed boundary layer vorticity. The net circulation was equal but opposite in sign to the shed vorticity.

The Second World War provided graphic evidence of the need to accurately predict weapon trajectories. To place a shell fired from a gun on target usually required more than one shot. Corrections were made from previous impacts to achieve the desired results. Significant reduction in the number of firings, time, and cost could be made if a weapon's trajectory could be accurately predicted.

In 1953 Martin [6] published the first analytical method for predicting Magnus forces developed by spinning

open-ended cylinders of revolution at small angles of attack in incompressible laminar flow. Kelly [7] followed in 1954 with a more detailed discussion of Martin's theory. Power [8], in 1971, carried Kelly's theory to a high order of approximation and included inviscid circulation development to obtain an equation for Magnus force coefficient. He improved previous theories by estimating shed vorticity that lies close to the body using a cross-flow analogy. This theory best models the essential Magnus force contributions and was used to correlate the wind tunnel data.

Martin, Kelly, and Power all developed their theories by studying open-ended cylinders. Kelly noted in his work that there were no known measurements with which he could compare his results and that his theory was not directly applicable to bodies with different nose shapes. Testing open-ended cylinders in a flow is impractical and nearly impossible because there is no method to suspend the body in the flow and spin it without complicated flow-disturbin equipment. For this reason all the testing that is described in this paper was done using a cylinder with an ogive nose shape. The ogive forebody shape was selected because of its constant surface curvature which allows theoretical boundary layer calculations to be made more easily.

MAGNUS FORCE PRODUCTION ON SLENDER BODIES OF REVOLUTION AT LOW ANGLES OF ATTACK

To study three-dimensional flow about a spinning body of revolution the full viscous equations of motion must be solved. The general equations of motion predict that the side force is a function of angle of attack, non-dimensional spin rate (the ratio of the surface speed ωr and the free-stream velocity U), body fineness ratio, Reynolds number, and Mach number. The complete equations of motion are much too difficult to solve, hence simplifications must be made. The simplest problem involves incompressible flow with a laminar boundary layer, a small angle of attack, and a small non-dimensional spin rate.

A useful method for studying such a flow is by using a cross-flow analogy. The basic assumption made to simplify the problem is that the flow along the body is independent of the flow across the body. This assumption is most likely inaccurate for high angles of attack and low body fineness ratios. Experimental test data, however, should define the region of validity for the application of this theory.

Using the cross-flow analogy, a spinning missile placed in a flow at an angle of attack is assumed to have the flow velocity about it resolved into two components as shown in Figure 1.

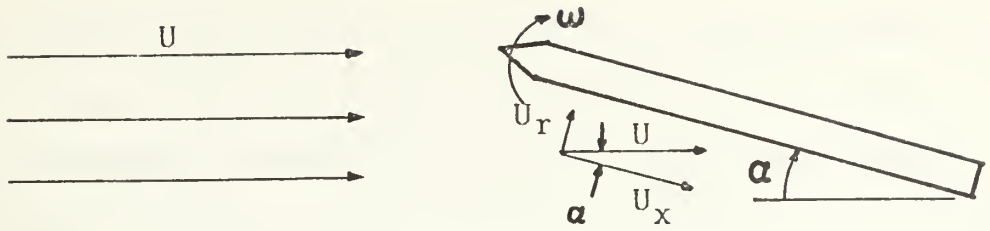

Figure 1. Velocity Components over a Spinning Missile

The drift experienced by the missile during flight can be explained by investigating the effect of the cross-flow component (the velocity component perpendicular to the missile).

From inviscid flow theory it is known that lift per unit span on a spinning cylinder in a uniform stream is

$$L = \rho U \Gamma .$$

where Γ is the circulation of the flow. The flow pattern for the spinning cylinder in inviscid flow is shown in Figure 2.

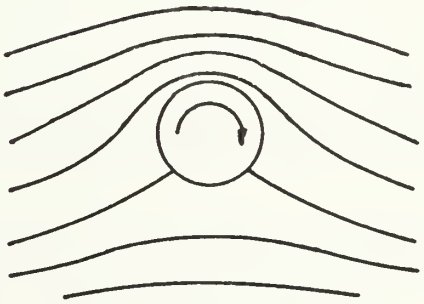

Figure 2. Streamline Pattern of a Spinning Cylinder in Inviscid Flow

Inviscid flow theory is helpful for understanding how lift is generated on a body in a flow, but it ignores how the circulation responsible for the lift is generated.

Real flow is viscous and does not behave as described in inviscid flow theory near the body surface. From boundary layer theory it is known that the flow around a spinning cylinder forms a boundary layer. This boundary layer is ultimately shed somewhere on the rear side of the cylinder in the flow. Because of the cylinder's rotation, the boundary layer formed is not symmetric about the cylinder nor is it shed symmetrically in the flow. The boundary layer is shed in the form of vortices and is shown schematically in Figure 3.

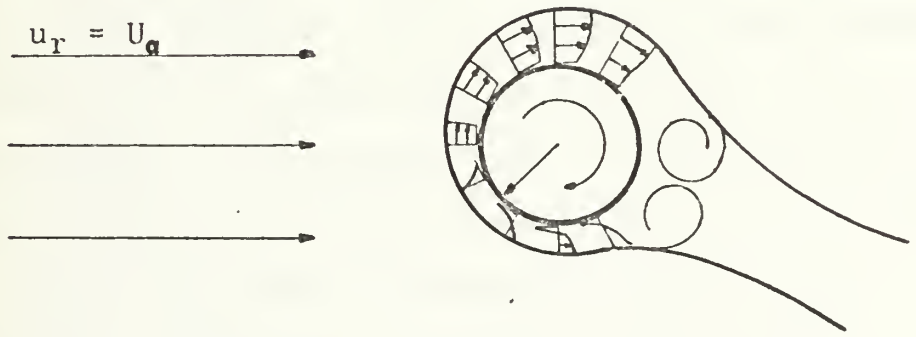

Figure 3. Boundary Layer and Shed Vorticity for a Spinning Cylinder in Inviscid Flow

The net vorticity is in the direction opposite to the rotation of the cylinder, in this case counter-clockwise. Because the total vorticity must be zero for the flow as a whole, a circulation in the clockwise direction is generated and it is this circulation which provides a

major contribution to the Magnus force acting on the cylinder.

In addition to the circulation, boundary layer displacement thickness, radial pressure gradient in the boundary layer, and the presence of skin friction shearing stresses contribute to the production of a Magnus force. The displacement thickness is the distance by which the boundary layer would have to be displaced if the entire flow were imagined to be frictionless. A representation of the displacement thickness is shown in Figure 3. It is not symmetric about the cylinder because of the effect the cylinder's spin has on the boundary layer growth. Knowledge of the displacement thickness permits use of a "displaced" body in place of the actual body such that the flow around the body can be considered frictionless. As can be seen in Figure 3, the magnitudes of the velocity components at the boundary layer edge of the advancing sid of the cylinder are less than those of the retreating side and hence the outer inviscid flow velocity is less below the cylinder than above. Because this outer flow is frictionless, Bernoulli's equation predicts that the pressure below the cylinder is less than that above, and a lift is generated.

Although small, it can be shown that there is a radial pressure gradient in the boundary layer around the cylinder due to the surface curvature. When integrated, the change

in surface pressure due to this pressure gradient contributes to the cylinder's lift.

The presence of friction on the surface of the cylinder is also a cause of lift. When the frictional shearing stress is integrated over the cylinder's surface there is a component of the resultant force in the direction of lift.

Although circulation is a major factor in creating lift on the spinning cylinder, the effects of the radial pressure gradient and surface friction, however small, should be included in the analysis of the total Magnus force developed by the cylinder.

DESCRIPTION OF APPARATUS

Testing to obtain experimental force data was done in the Naval Postgraduate School low speed wind tunnel. The tunnel test section was hexagonal in shape with maximum dimensions of 3.5 x 5.0 feet.

The model used for testing was a five-sectioned aluminum cylinder 2.950 inches in diameter with an ogive nose shape as shown in Figure 4. The missile was constructed in sections so that length-to-diameter ratios of 9.9, 7.8, and 6.0 could be tested.

Figure 5 is a line drawing of the model and sting balance system. The missile was supported by two Fafnir KD66 precision ball bearings which were press-fitted onto the sting balance. Each bearing was enclosed in a stainless steel collar which allowed the missile to be fastened to it with screws. Mounted at the end of the balance was a 1/8 horsepower Standard Pneumatic rotary-vane, bi-directional compressed air motor. Figure 6 shows the balance, bearing, and motor configuration. The compressed air was supplied to the motor through 1/4-inch copper tubing routed along the missile support apparatus.

Mounted on the drive shaft of the air motor was an aluminum drive disk. Located near the disk was an electromagnetic tachometer pickup which sensed passage of ferrous material (steel screws) in the aluminum disk.

Figure 4. Test Model at Positive Angle of Attack

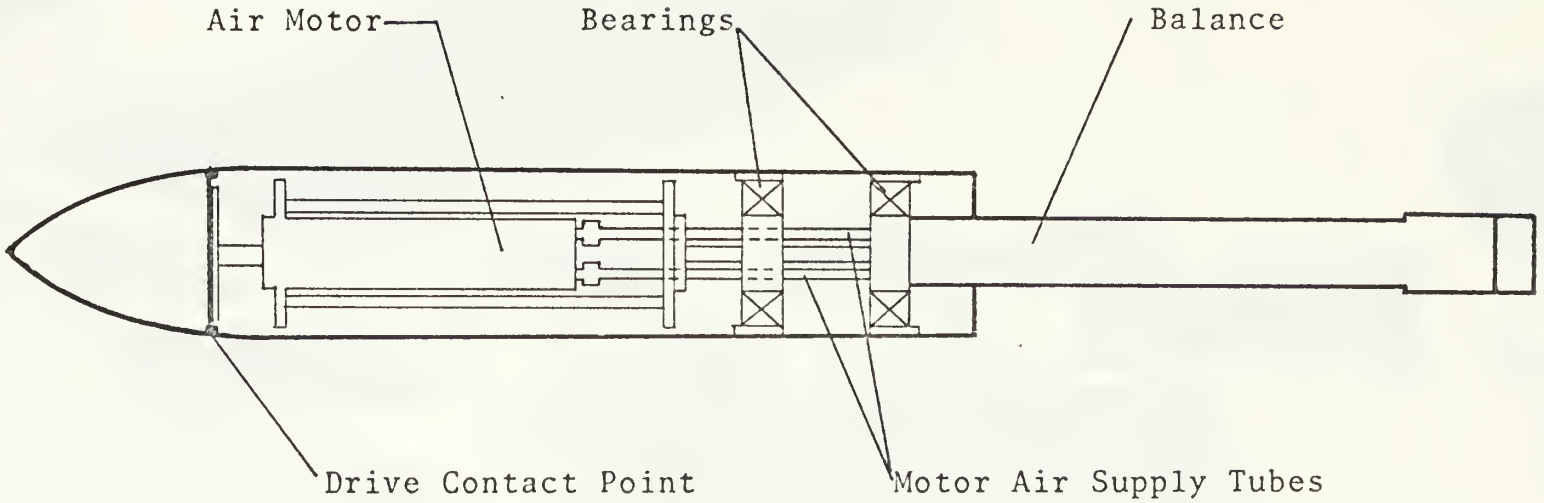

Figure 5. Details of Model, Air Motor, and Balance

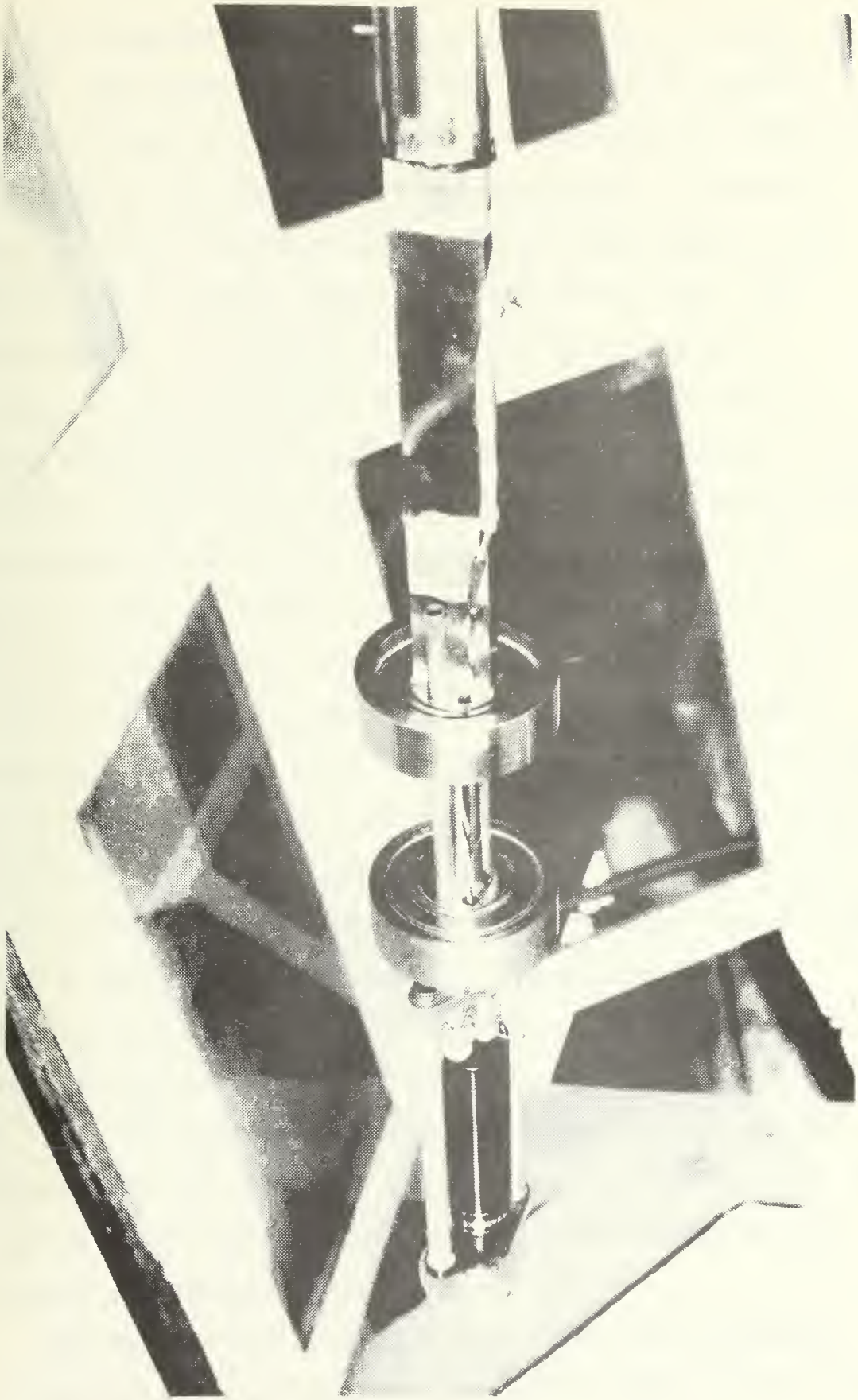

Figure 6. Balance, Bearing and Air Motor

Also mounted on the balance were two four-element strain gage bridge circuits which were used to measure strain in the sting balance and thus provide the means of determining the Magnus force and its center of pressure. Each gage was a Baldwin-Lima-Hamilton strain gage, model number FAE 25 12S13, with a gage factor of 2.08. The arrangement of the gages for one bridge is shown in Figure 7. The gages were wired in such a manner as to sense only side force and the Magnus moment applied to the balance. Because of the beam geometry and the longitudinal arrangement of the gages there was no response to any applied torque. Lift forces on the beam also had no effect on the bridge output because of gage arrangement. The bridge remained balanced when lift forces were applied because one pair of gages (#2 and #4 as shown) was in compression while the other pair (#1 and #3) was in tension. The currents in each pair were different because resistances were different, but because the voltage drop was the same across each pair the bridge remained balanced. Because each bridge circuit was made up of four active elements the strain indication was magnified by a factor of four. The bridge was also temperature compensating because all elements were affected the same by changes in temperature. Figure 8 is a picture of one side of the balance with mounted strain gages.

The balance was screwed at its base into a tapered, circular cross-section, stainless steel sting. The sting

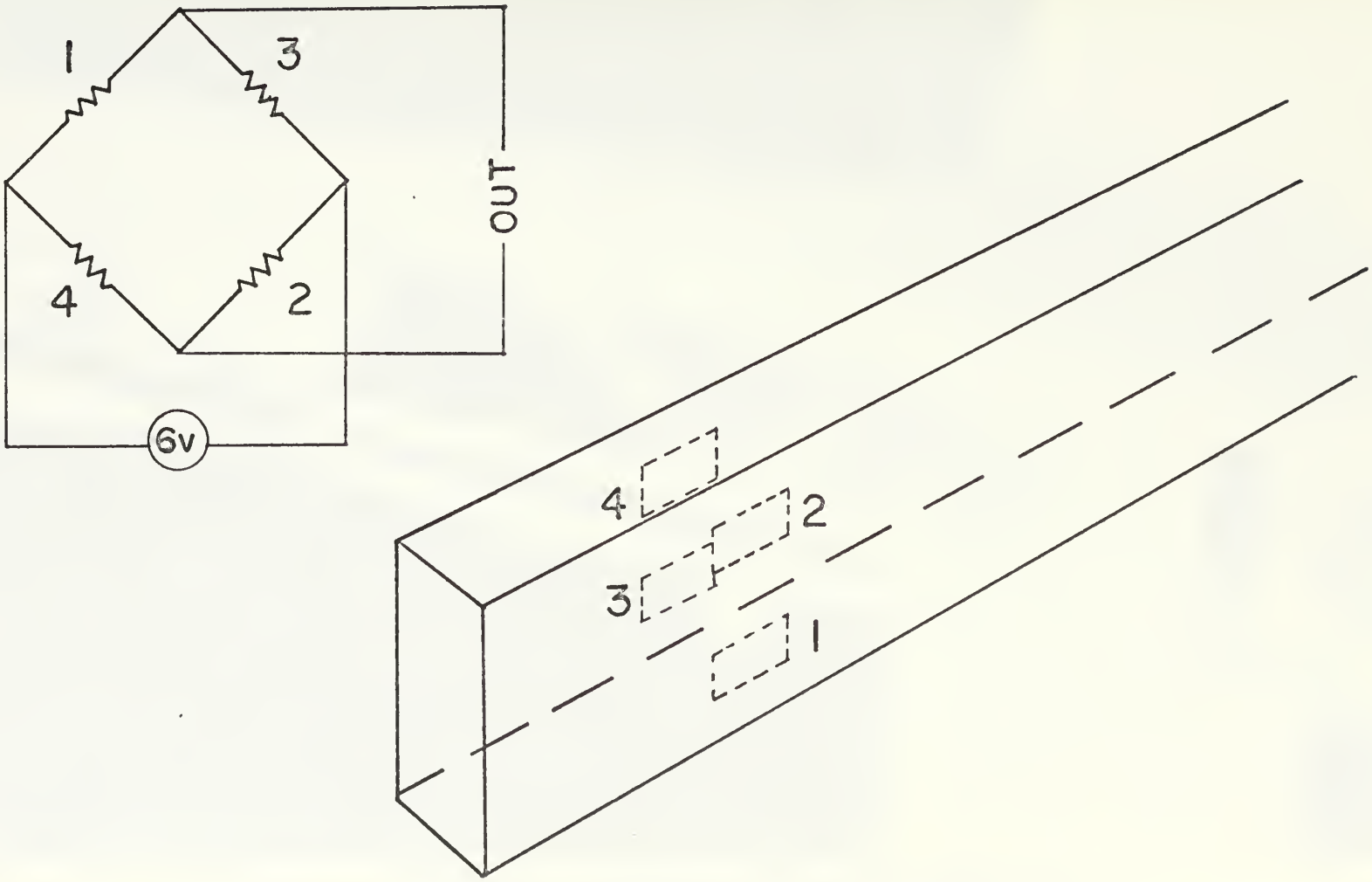

Figure 7. Balance Bridge Circuit Configuration

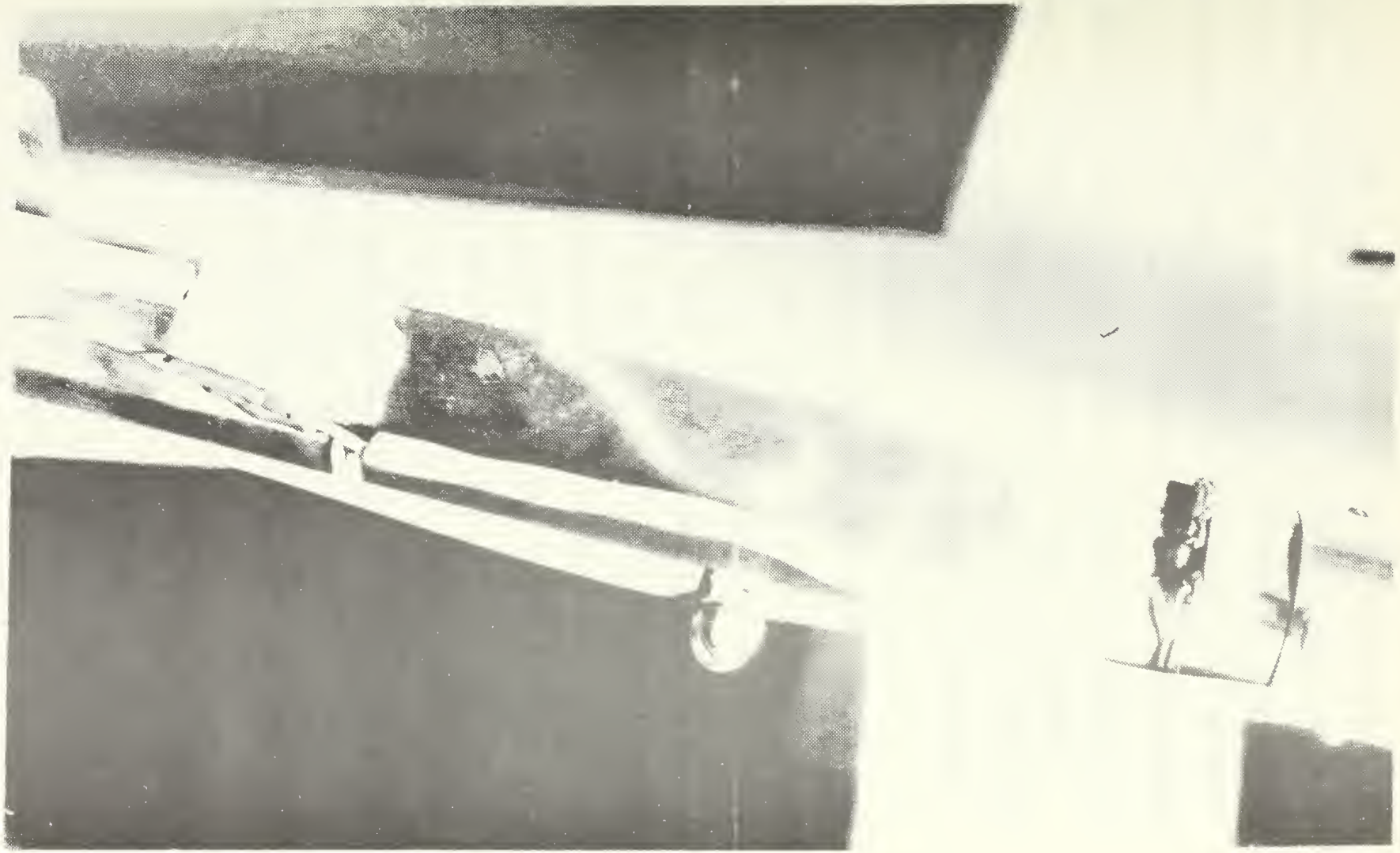

Figure 8. Balance and Strain Gages

was held in place at its base by a support and could be rotated 90° for measurements in either the horizontal or vertical plane. A 90 x 6 x 1-inch aluminum sting support was bolted top and bottom to the wind tunnel to support the missile and sting arrangement. The beam was machined so that the entire sting could be rotated in the vertical plane to provide angle of attack as shown in Figure 4. The sting support was raised or lowered to keep the model centered in the test section. The angle of attack was measured with a clinometer.

Figure 9 is a wiring diagram of the electronics used to obtain data. An input voltage of 6 volts was supplied to each bridge circuit by a Moxon Electronics SRC Division power supply, model 3564. Each bridge output was amplified by a factor of 100 by an Aztec model 886 DC amplifier and recorded on a Hewlett-Packard two channel chart recorder, model 7100B. Two potentiometers per bridge circuit were used to initially balance each bridge before testing was begun. Figure 10 is a picture of the apparatus used in the testing. In addition to the digital counter, a General Radio strobe, model 1540-P1, was also used to determine missile spin rate to the nearest 10 RPM.

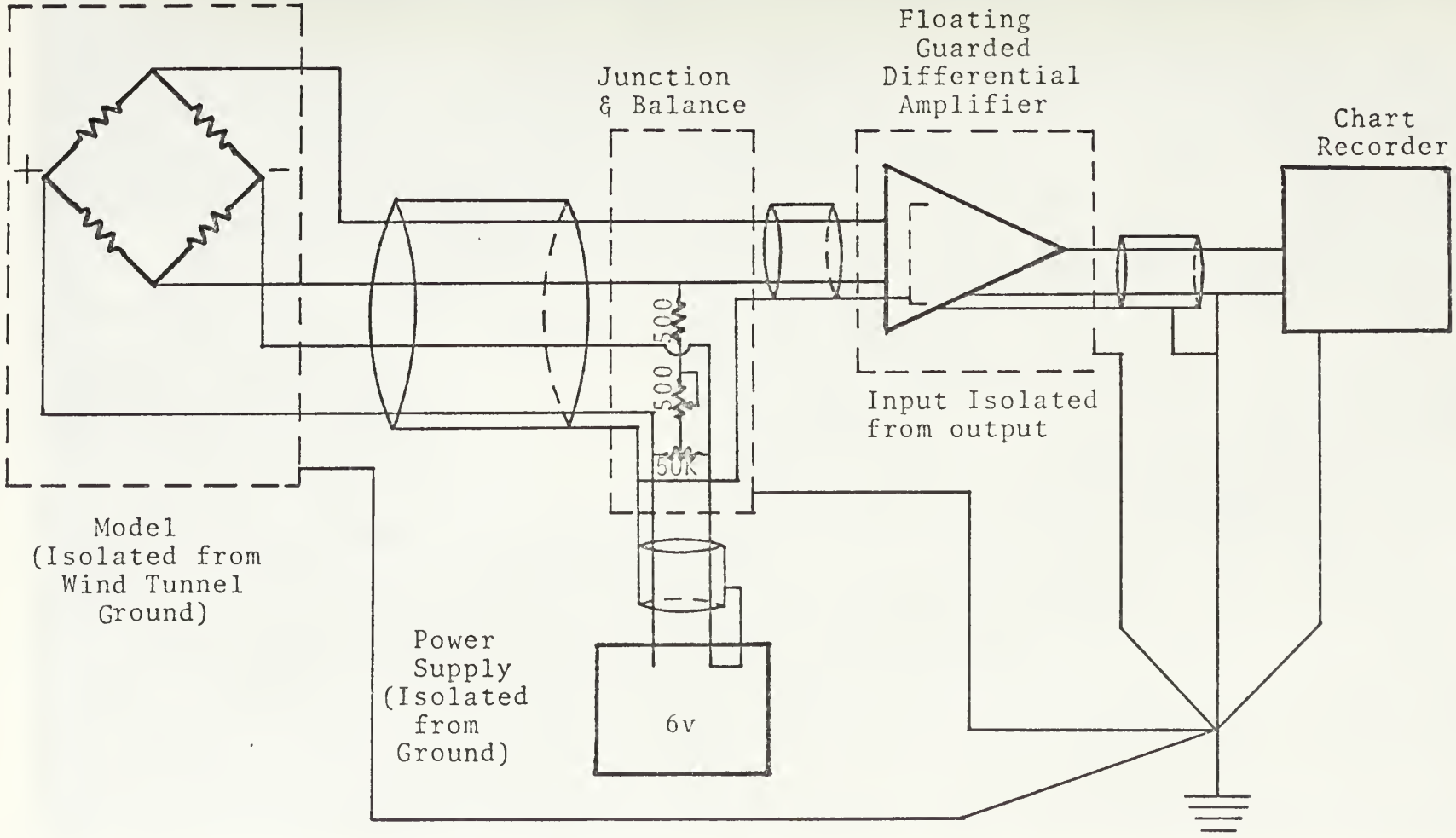

Figure 9. Wiring Schematic for Electronic Equipment

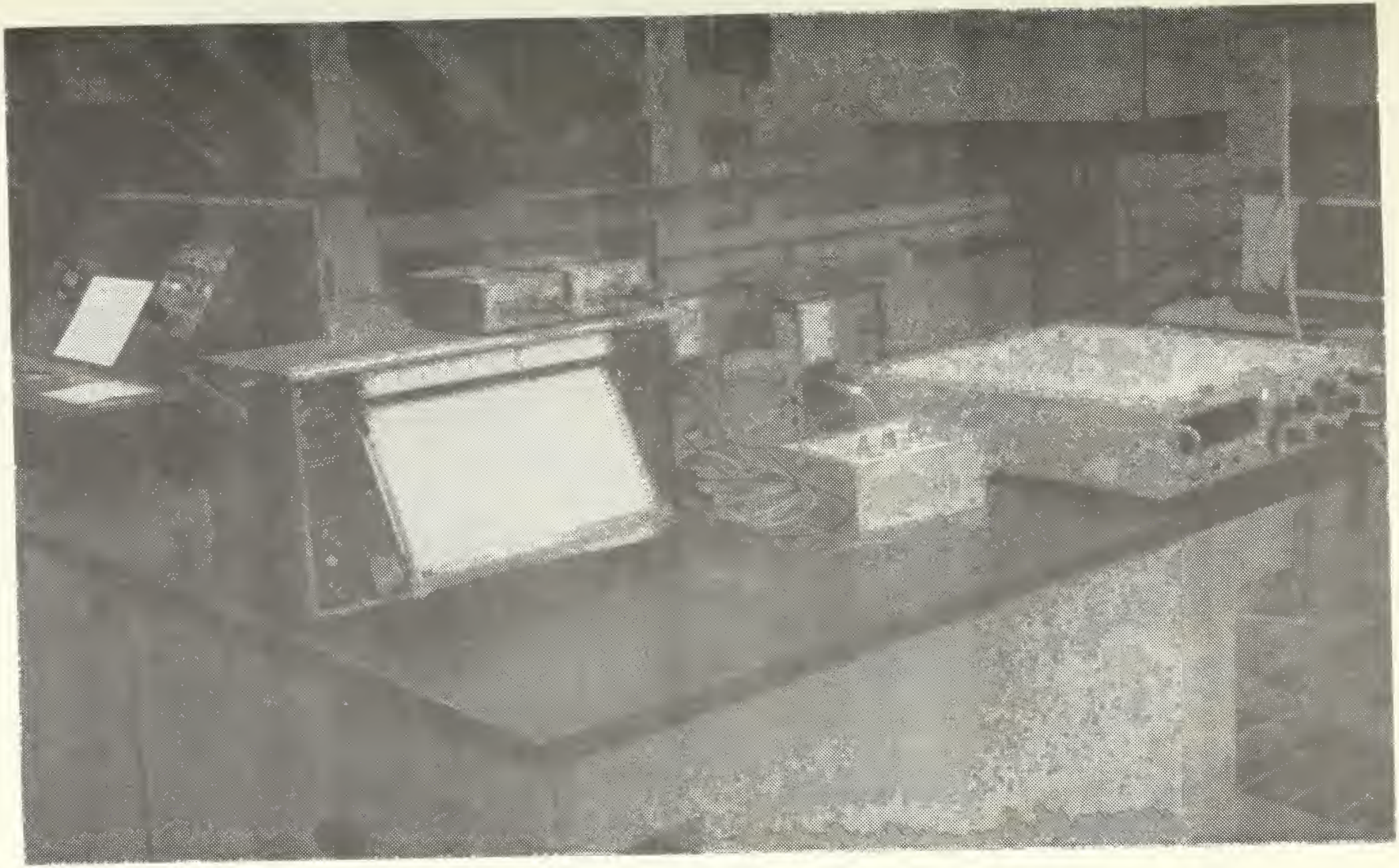

Figure 10. Electronic Equipment

CALIBRATION AND DATA REDUCTION METHODS

Airspeed in the tunnel test section was measured using water manometry. A pitot tube which measured total and static pressures in the test section provided the inputs to the water manometry set up. Because the pitot tube was located in the most forward part of the test section and only six inches off the test section's floor, calibration of the system was necessary. To calibrate the tunnel's system another pitot tube was mounted in the center of the test section and readings were compared throughout the range of airspeeds possible in the tunnel. These corrections to tunnel readings were made in the computer data reduction program.

In addition to pitot tube calibration, corrections to the test section velocities were necessary due to test section blockage by the model. The correction applied is developed in Pankhurst and Holder [9]:

$$V_{true} = V_{obs}(1.0 + \epsilon_s)$$

where V_{obs} is the velocity directly measured in the tunnel test section, ϵ_s is the tunnel blockage factor and is given by:

$$\epsilon_s = (\frac{\pi}{4})^{\frac{1}{2}} \tau (1.0 + .4D/L) \frac{Vol}{C^{3/2}}$$

where $(\frac{\pi}{4})^{\frac{1}{2}}$ is a factor appropriate to a body of revolution, τ is a factor dependent on the shape of the tunnel

cross section, Vol is the volume of the model, D/L is the reciprocal of the model fineness ratio, and C is the tunnel test section cross sectional area.

Corrections to test data due to the effect of air hose pressurization on bridge circuit output were necessary. Pressure applied to the air motor stiffened the rubber hoses leading to the motor and caused a deflection in the sting balance which in turn affected strain gage bridge output. Corrections for pressurization were made in the computer data reduction program to correct for these effects. Input data for the pressurization corrections were obtained by prior calibration of the sting balance which gave chartline deflection for any given air pressure.

The sting balance system described previously was calibrated by hanging a known weight a known distance from each bridge circuit location and recording each bridge's output in units of chart lines on the Hewlett-Packard chart recorder. Calibration apparatus is shown in Figure 11. By plotting the moment versus chartline deflection for each bridge circuit linear graphs were obtained whose slopes were calculated. Test results (chartline deflections for unknown forces) were multiplied by the slopes for each circuit to determine moments. By knowing the moment at each bridge circuit the applied force and its location as shown in Figure 12 were calculated using the following simultaneous algebraic equations:

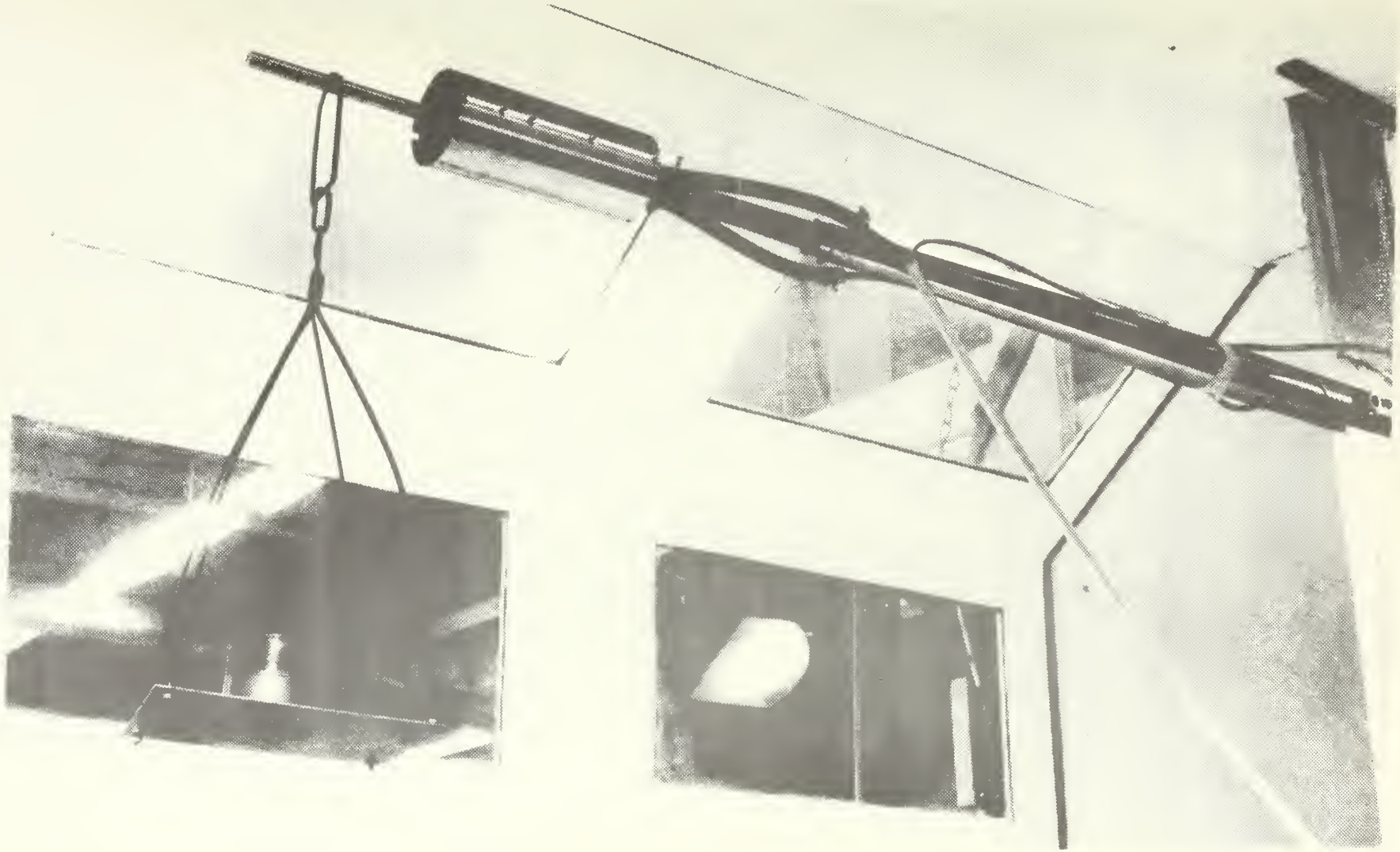

Figure 11. Calibration Rig

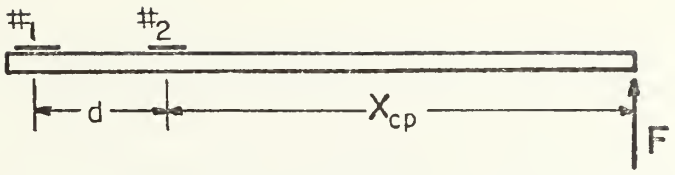

Figure 12. Strain Gage Bridge/Beam Geometry

$$F = (M_1 - M_2)/d$$

$$X_{cp} = M_2/F$$

TESTING PHILOSOPHY AND PROCEDURE

Testing to determine the Magnus moments was done with the objective of obtaining data to verify the theoretical equation developed by Power in 1971 [8], which predicts the Magnus force coefficient developed by a spinning body of revolution. Power's equation showed that the Magnus force coefficient was dependent on angle of attack, non-dimensional spin rate (ratio of Cylinder surface speed to flow velocity), model length-to-diameter ratio, the Reynolds number based on missile length, and the cross flow Reynolds number.

$$C_Y = \frac{\alpha \bar{p}_{1/2}}{R_L} \left(\frac{L}{D}\right)^2 \left\{ 60.9757 + \frac{1_{1/2}}{R_L} \left(\frac{L}{D}\right) \left[256\, C_1\, R_C^{3/4} - 357.37 \right] - \frac{227.0112}{R_L} \left(\frac{L}{D}\right)^2 \right\} \qquad (1)$$

where $C_1 = \frac{.6\alpha f}{128 \pi \bar{p}}$ and f, given in Figure 12, is a functio of cylinder spin rate and angle of attack. By varying angle of attack, non-dimensional spin rate, and the model length-to-diameter ratio while maintaining constant Reynolds numbers for each angle of attack, data could be obtained for three length-to-diameter ratios and various spin rates which would enable the theoretical equation to be compared with experimental data. Because the non-dimensional spin rate was in part dependent upon the Reynolds number based

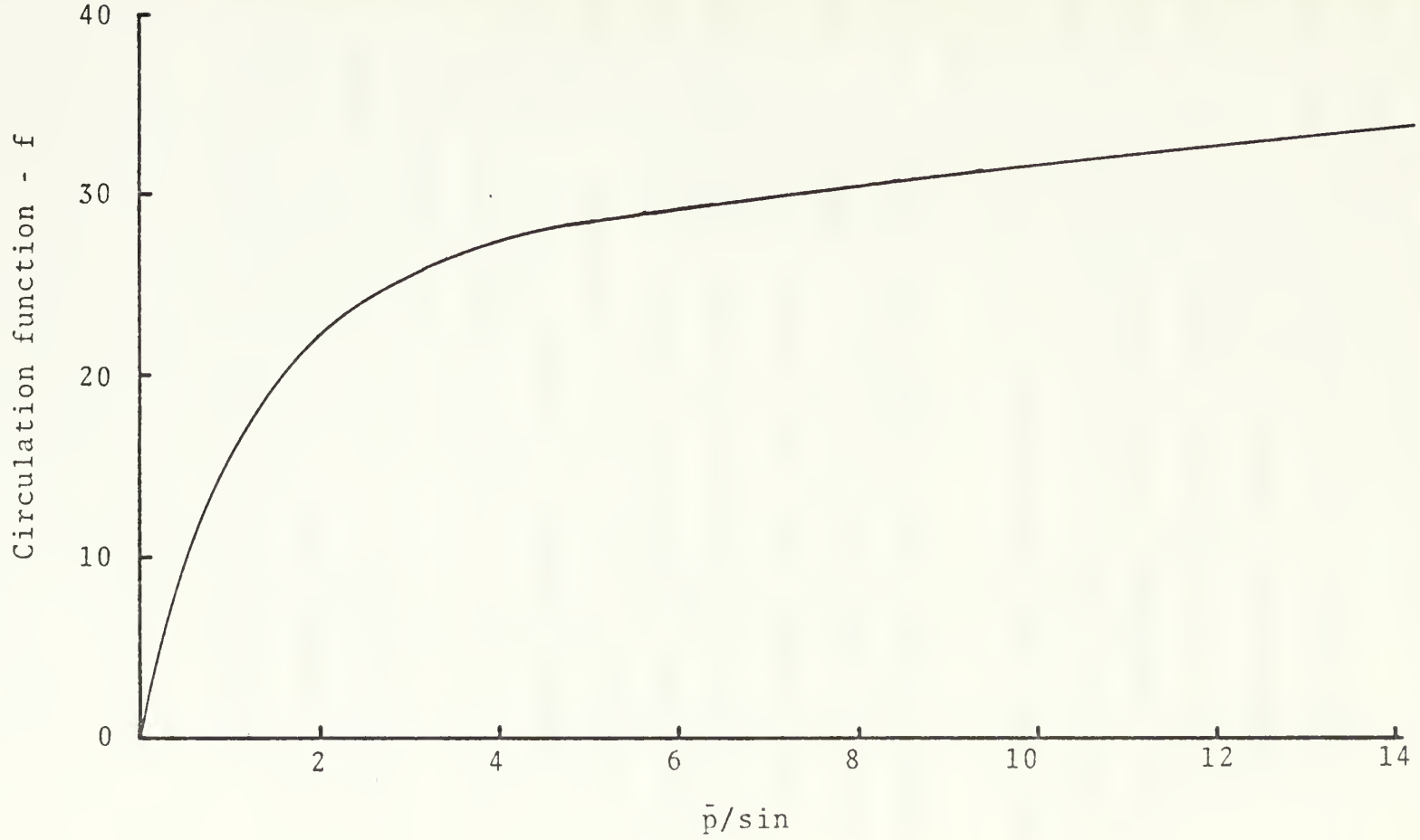

Figure 13. Circulation function for spinning cylinders

on model length, two Reynolds numbers were chosen for testing which were compatible with all three model lengths and wind tunnel capabilities. The two Reynolds numbers selected were 700,000 and 1,600,000.

It was found that pre-determining non-dimensional spin rate ($\bar{p}$) for the given Reynolds number was impractical because the spin rate required for each $\bar{p}$ was difficult and time-consuming to set during testing. Therefore, the procedure decided upon was to pre-select various air pressures to the air motor and accept whatever spin rates and hence $\bar{p}$'s that resulted.

Procedure played a major part in the testing because of the time that could be saved through proper planning. Because two tunnel velocities and a wide range of non-dimensional spin rates (plus and minus) were tested for each angle of attack, testing was extremely time consuming. By establishing a procedure which involved a minimum number of configuration, tunnel velocity, and model spin rate changes, the time consumed for any part of the testing was reduced to a minimum.

Upon completion of testing all raw data obtained were typed on computer cards and fed into an IBM 360 digital computer and reduced by the data reduction program.

DATA ANALYSIS

Due to various physical phenomena encountered during the testing the raw data obtained were very difficult to analyze to obtain meaningful results. A sample of the type of data obtained during the testing from the Hewlett-Packard chart recorder is shown in Figure 14.

The raw data indicated that the missile vibrated in two modes during the testing. The amplitude of the short period mode varied between three and five chartlines (three and five millivolts) and appeared to be at a constant frequency throughout the testing. The amplitude of the long period mode varied between eight and eleven chartlines in amplitude (measured from the mean of the short period oscillation) but its frequency was random.

Data were obtained by considering the long period mode first. The best estimate of its average amplitude was made and this information was modified, if necessary, by considering the superimposed average short period amplitude. In this way a constant voltage value was determined for use in the data reduction program. Because of the constant frequency of oscillation of the short period mode, averaging was easy compared to averaging the random oscillations of the long period mode. These vibrational modes were caused by at least four major effects. First, tunnel wall vibration was transmitted to the model through the model

Figure 14. Sample of Raw Data Output

support system. The sting and support were bolted directly to the tunnel floor and ceiling in the test section. Lack of time prevented the construction of the originally designed isolated support system. Second, mass unbalance of the missile itself caused a vibration when the missile was rotating. Even though the missile and bearing collars were finely machined there was a mass unbalance due to varying missile wall thickness and bearing slop. Third, asymmetric vortex shedding and leeside separation of the flow about the missile added to the vibration. This was a function of Reynolds number and rotation rate. Fourth, the tunnel test section velocity was not constant and large air flow fluctuations occurred. The solution to this problem would be to install flow-straightening screens to the tunnel to ensure constant low turbulence flow in the test section.

During the testing a breakdown forced the removal of one of the two counter-rotating Bendix constant speed propellers used to generate the tunnel's velocity. This severely reduced the maximum velocity that could be attained and subsequently delayed the testing programs until maintenance was completed and a new set of parameters for testing, reflecting the change in tunnel speed capability, could be computed. The removal of the propeller was necessary because of lack of parts. The long period of vibration was attributed primarily to the tunnel test section velocity fluctuations while the short period oscillations

were attributed to tunnel wall vibration, mass unbalance in the missile, asymmetric vortex shedding, and flow separation.

Because of the magnitude of the oscillations and tunnel flow variations, error bounds were computed. Due to the type of strip chart paper used (ten chart lines per inch) it was assumed that the raw data were accurate to within ±1 chartline. It was also estimated that tunnel flow fluctuation was ±1 centimeter of water at dynamic pressures above 10 centimeters of water and ±.5 centimeter below dynamic pressures of 10 centimeters. Evaluation of the error bound for each data point was done by computer analysis and representative values are shown in Figure 15. The error in C_Y due to tunnel velocity fluctuations was about 11% at each Reynolds number tested. The major error contribution was due to the vibration and the resulting inability to interpret the strain gage readings accurately. The uncertainty bound for each data point was computed by adding one chartline to the aft bridge circuit reading and subtracting one chartline from the forward bridge circuit reading. In this way the maximum testing error could be calculated. It can be seen in Figure 15 that the larger of these uncertainties occurred for the lowest Reynolds number and highest angles of attack (C_Y is directly proportional to angle of attack and inversely proportional to tunnel velocity). Because of the magnitude of the error

	L/D	Re(L)	$\bar{p}$	C_Y
0	6.0	7.0×10^5	.32	.02±.255
6	↓	↓	-.30	.19±.250
12			.24	-.03±.265
18			-.32	.15±.275
0	6.0	1.6×10^6	-.17	.03±.045
6	↓	↓	.13	.02±.050
12			-.10	.02±.045
18			.09	-.04±.045
0	7.8	7.0×10^5	-.45	-.01±.465
6	↓	↓	.13	.33±.460
12			-.10	.20±.445
18			.09	.38±.425
0	7.8	1.6×10^6	-.18	.09±.090
6	↓	↓	-.17	.08±.085
12			.16	.13±.080
18			-.14	.01±.080
0	9.9	1.6×10^6	.22	.17±.125
6	↓	↓	-.16	.18±.125
12			.17	.10±.120
18			.20	.12±.115

Figure 15. Maximum Error Bound Samples

bounds, interpretation of the data was very difficult. Similar problems have plagued all experimenters investigating Magnus forces to date. The forces measured are very small and the data accuracy required is better than that usually required for measuring drag forces.

RESULTS

A representative summary of the data obtained during experimentation is presented in tabular form in Appendix B and graphically in Figures 16 through 27. Figures 16 through 20 are plots of corrected data. At each angle of attack the data were reduced by subtracting the Magnus force coefficient obtained for the no-spin condition from each data point. This ensured that the curve of force coefficient versus spin rate would pass through the origin as predicted by theory. This procedure corrected the data for the experimental side force coefficient resulting from any missile yawing mis-alignment in the tunnel. Representative error bounds for the data points are shown for each of the first five plots (16 through 20). As discussed earlier, the bound is larger for the smaller Reynolds number and higher angles of attack. Small α and $\bar{p}$ theory predicts that a plot of C_Y versus $\bar{p}$ is linear. Hence the corrected data points in Figures 16 through 20 were fitted with a straight line whose slope $\partial C_Y/\partial \bar{p}$ was cross-plotted versus angle of attack for each length-to-diameter ratio and Reynolds number. This slope was then adjusted to yield a smooth variation for $\partial C_Y/\partial \bar{p}$ versus α. Justification for this method was provided by the size of the error bound in each case.

Figures 21 through 25 are the resulting plots of the Magnus force coefficient C_Y versus angle of attack α. Also shown are results developed by Power and Kelly for calculating Magnus force coefficients. Figures 26 and 27 are plots of Magnus force coefficient versus length-to-diameter ratios for constant Reynolds number and angle of attack and for various spin rates.

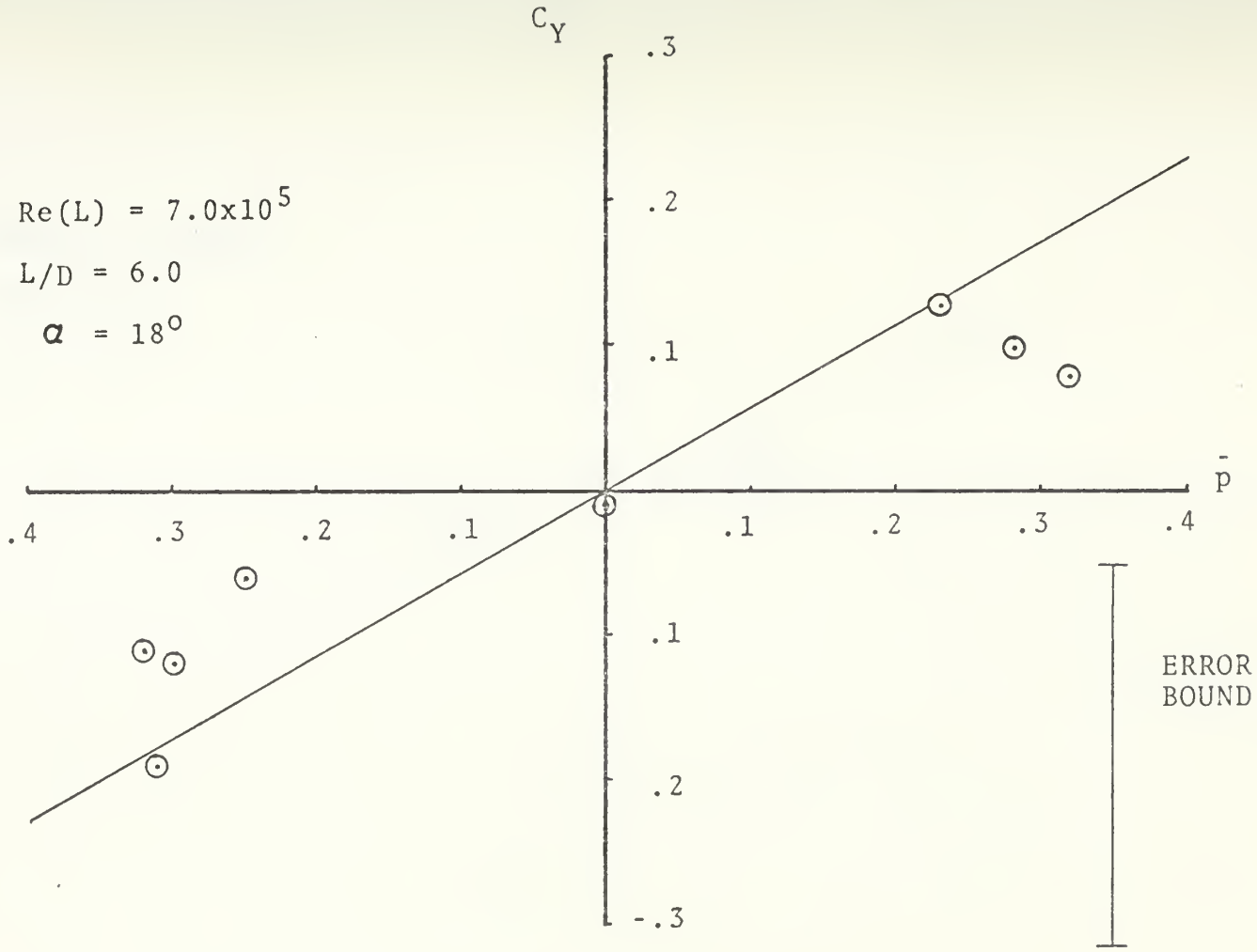

Figure 16. Magnus Force Coefficient vs. $\bar{p}$

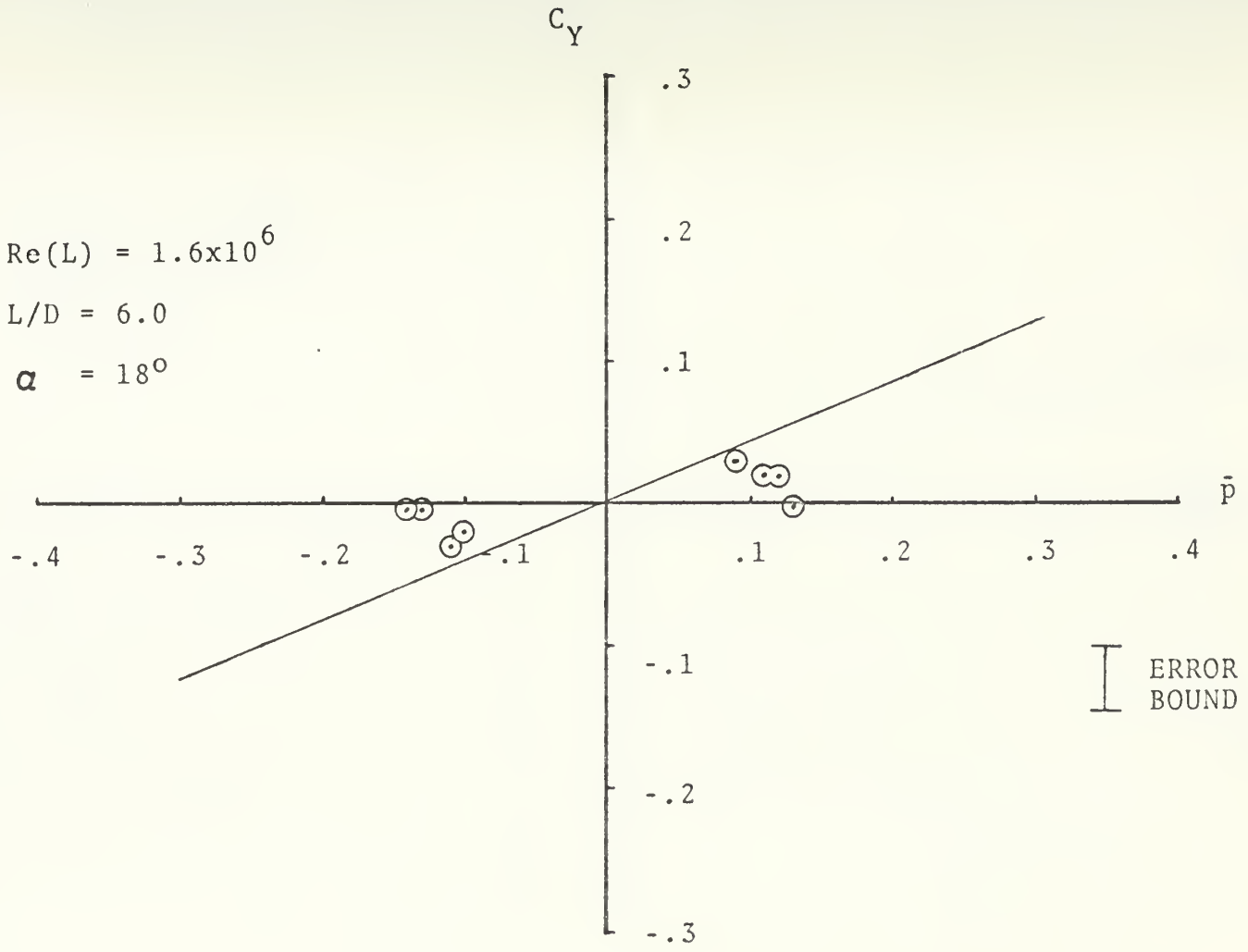

Figure 17. Magnus Force Coefficient vs. $\bar{p}$

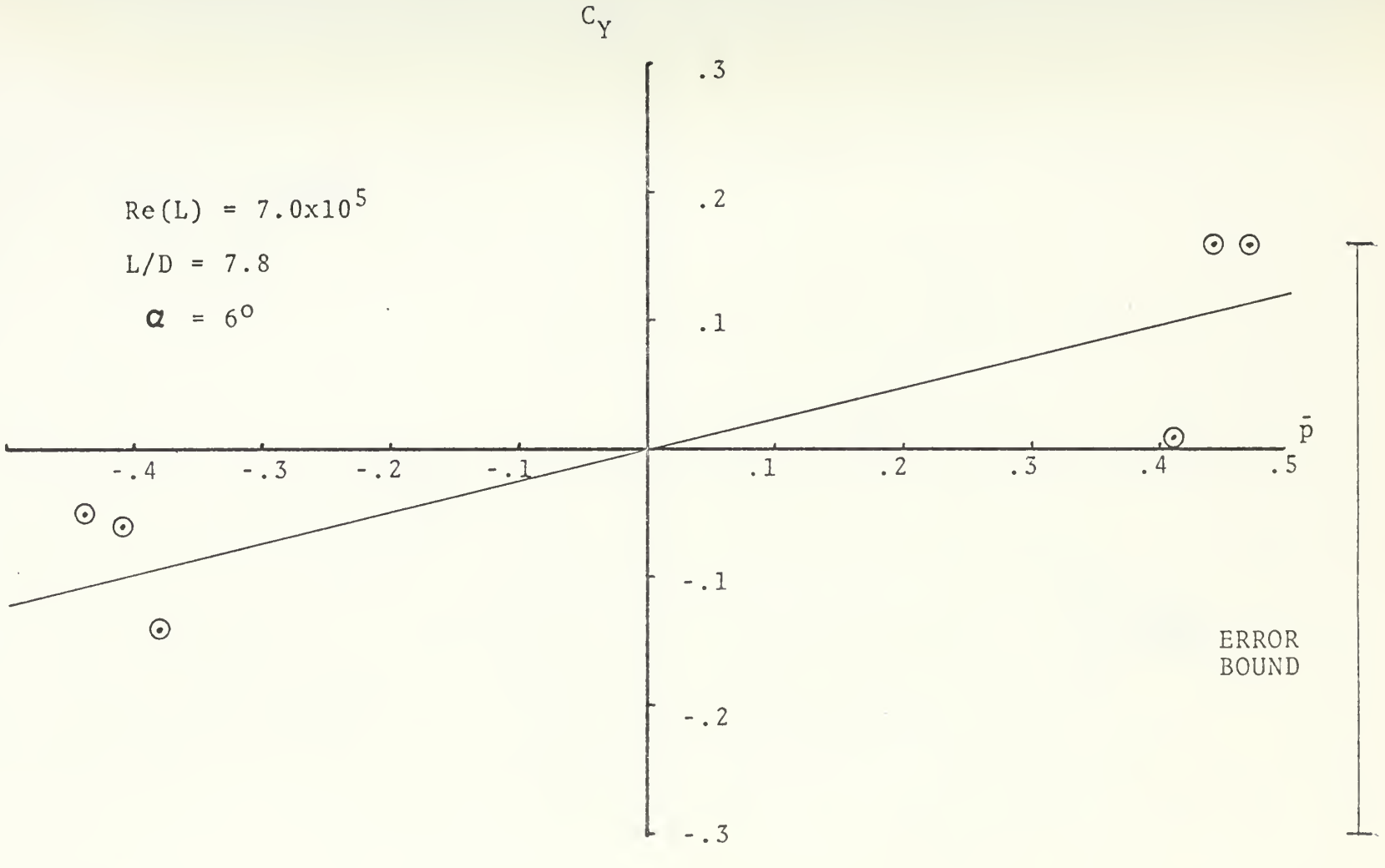

Figure 18. Magnus Force Coefficient vs. $\bar{p}$

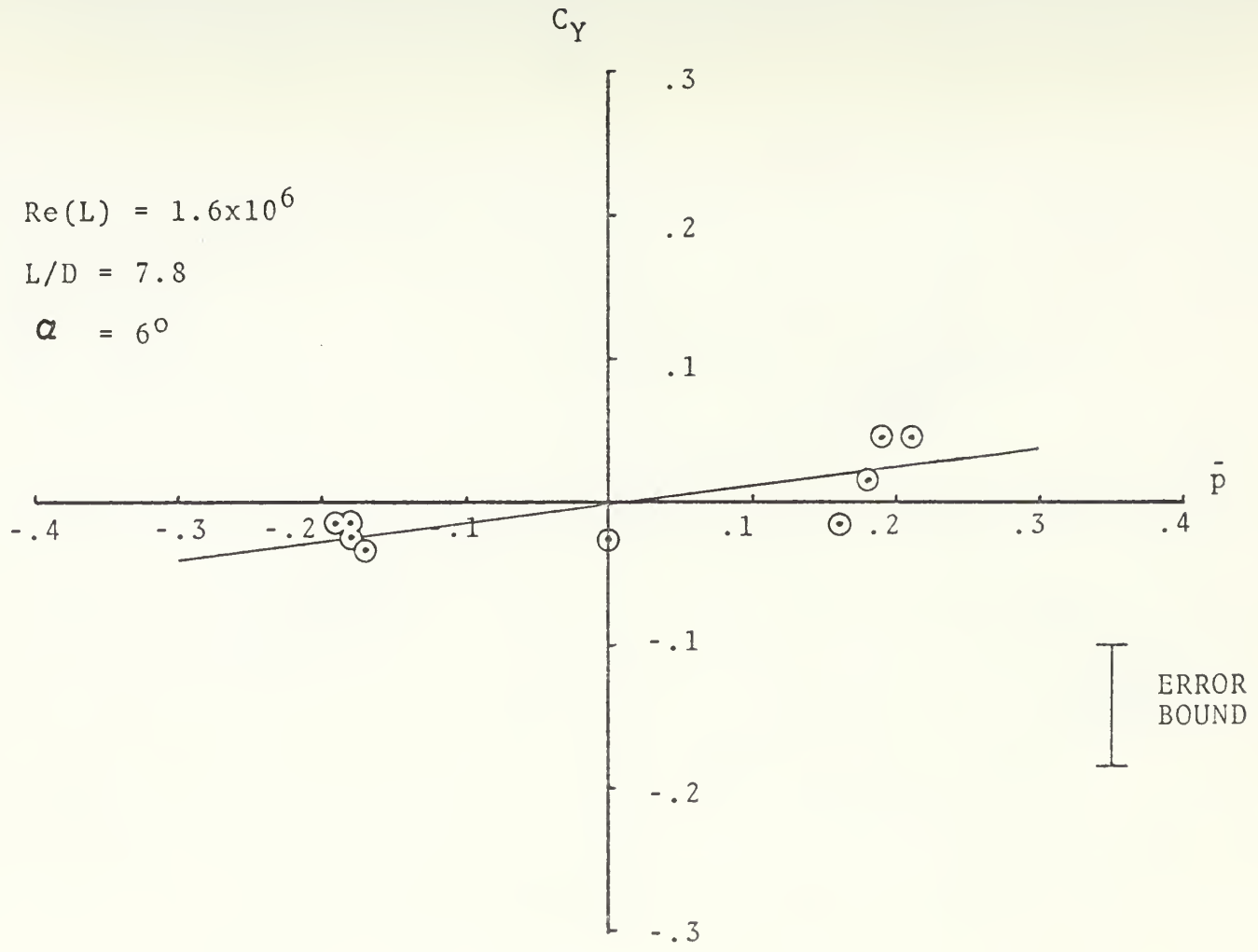

Figure 19. Magnus Force Coefficient vs. $\bar{p}$

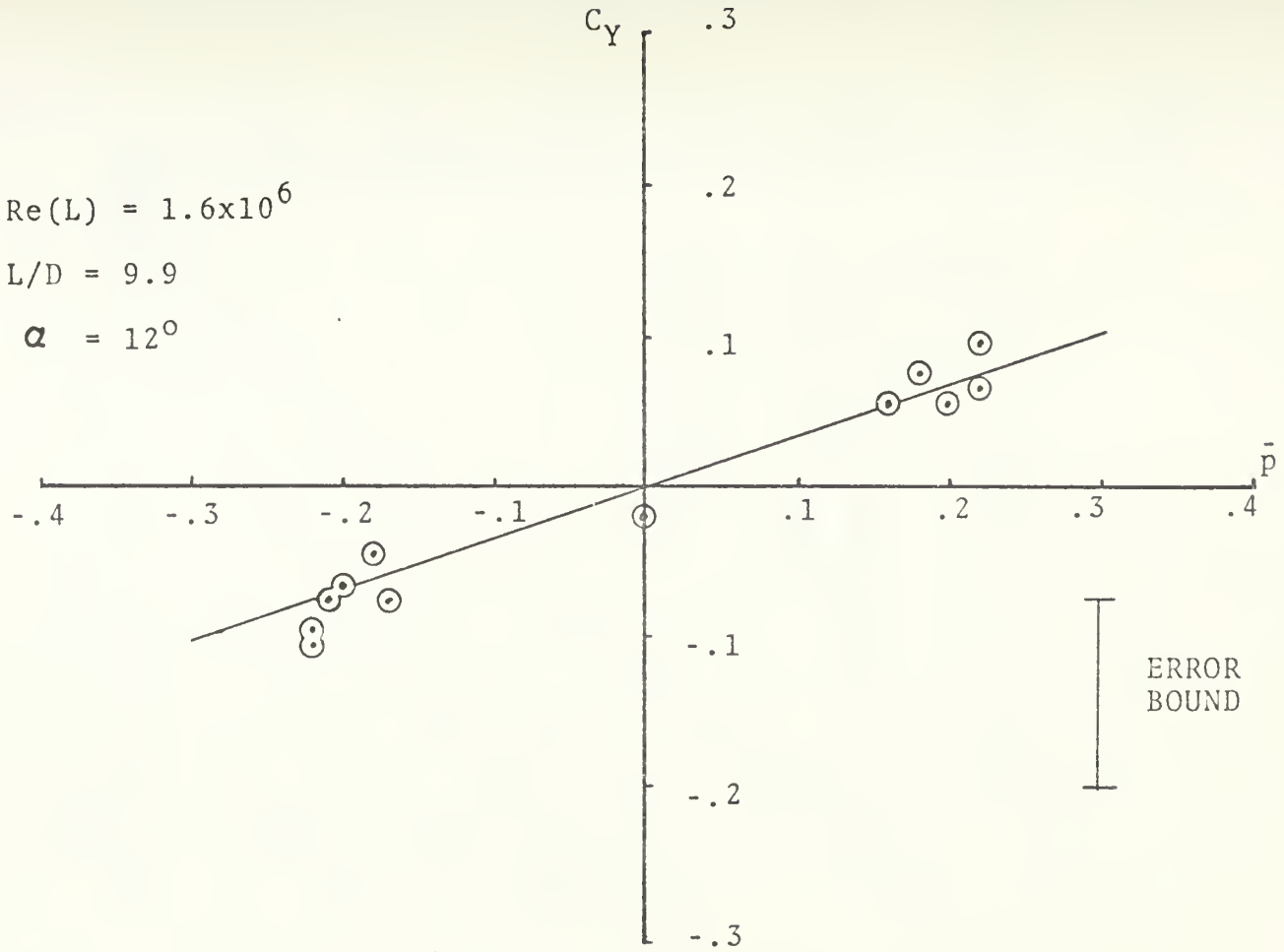

Figure 20. Magnus Force Coefficient vs. $\bar{p}$

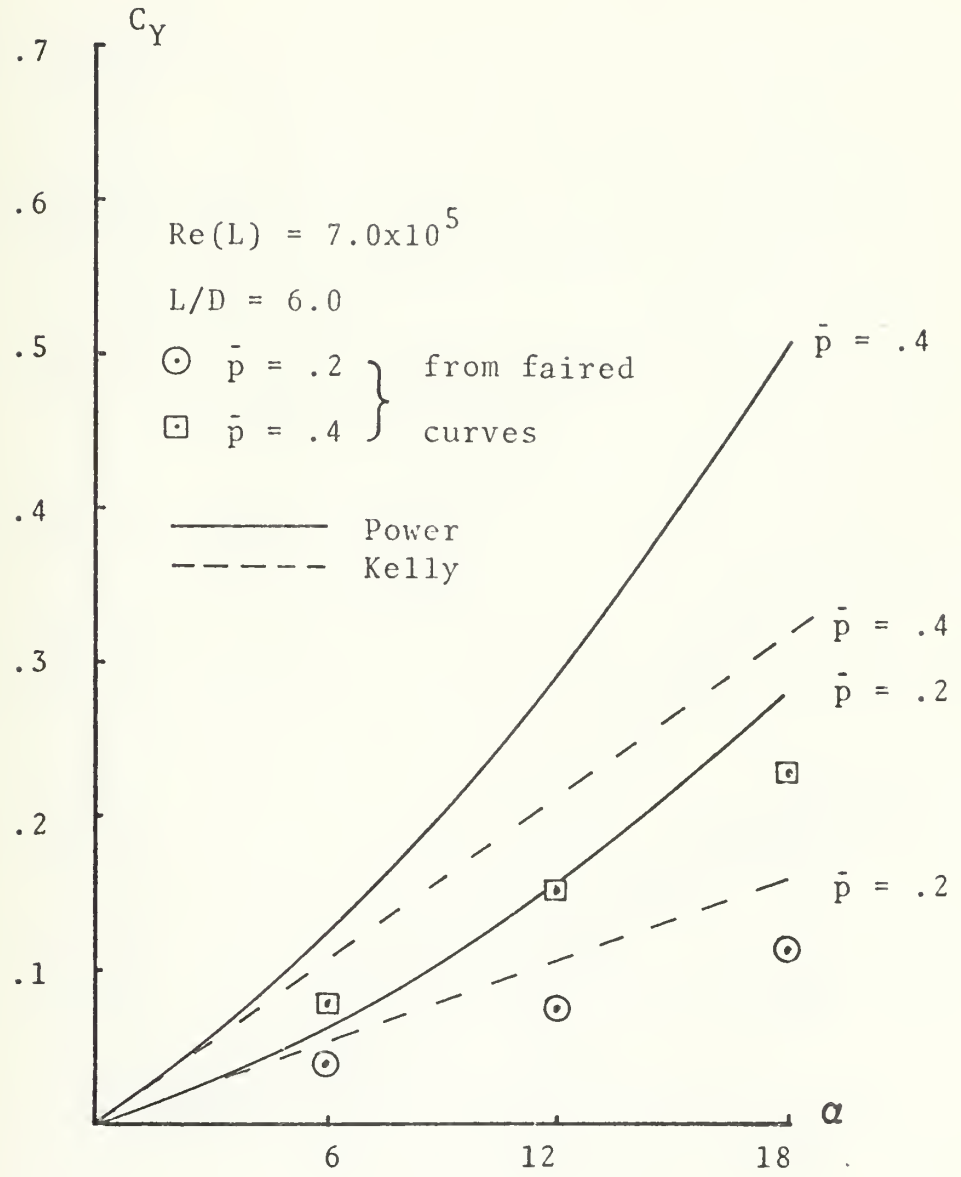

Figure 21. Magnus Force Coefficient vs. Angle of Attack

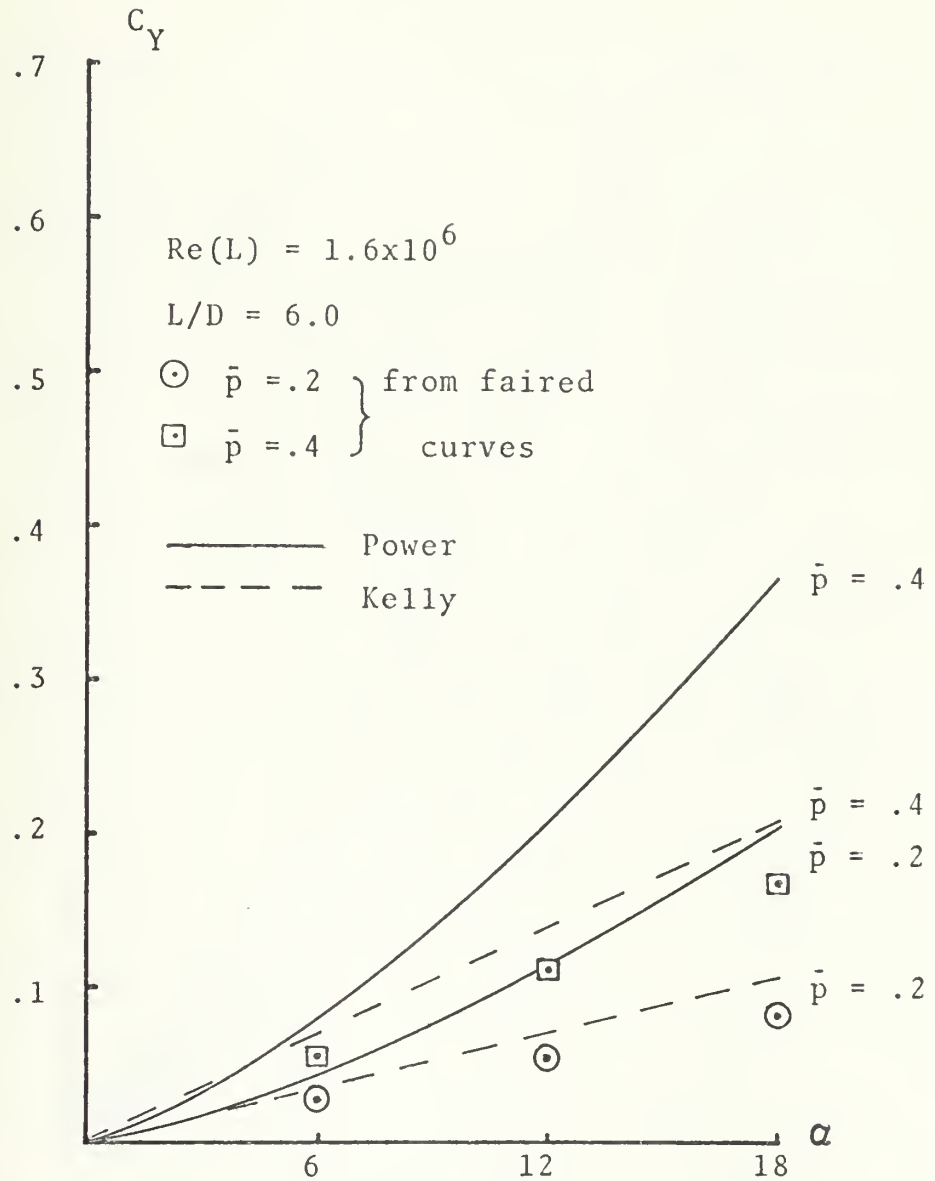

Figure 22. Magnus Force Coefficient vs. Angle of Attack

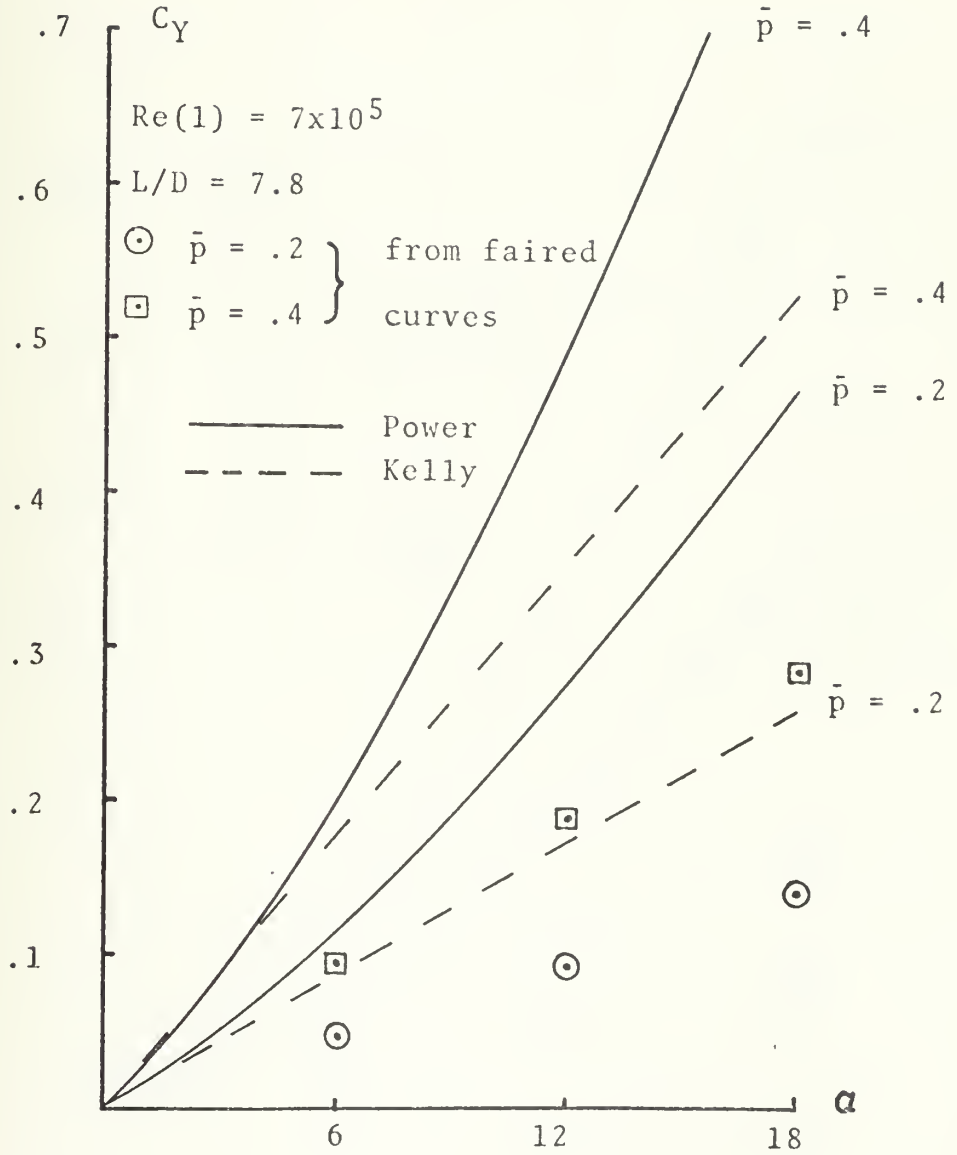

Figure 23. Magnus Force Coefficient vs. Angle of Attack

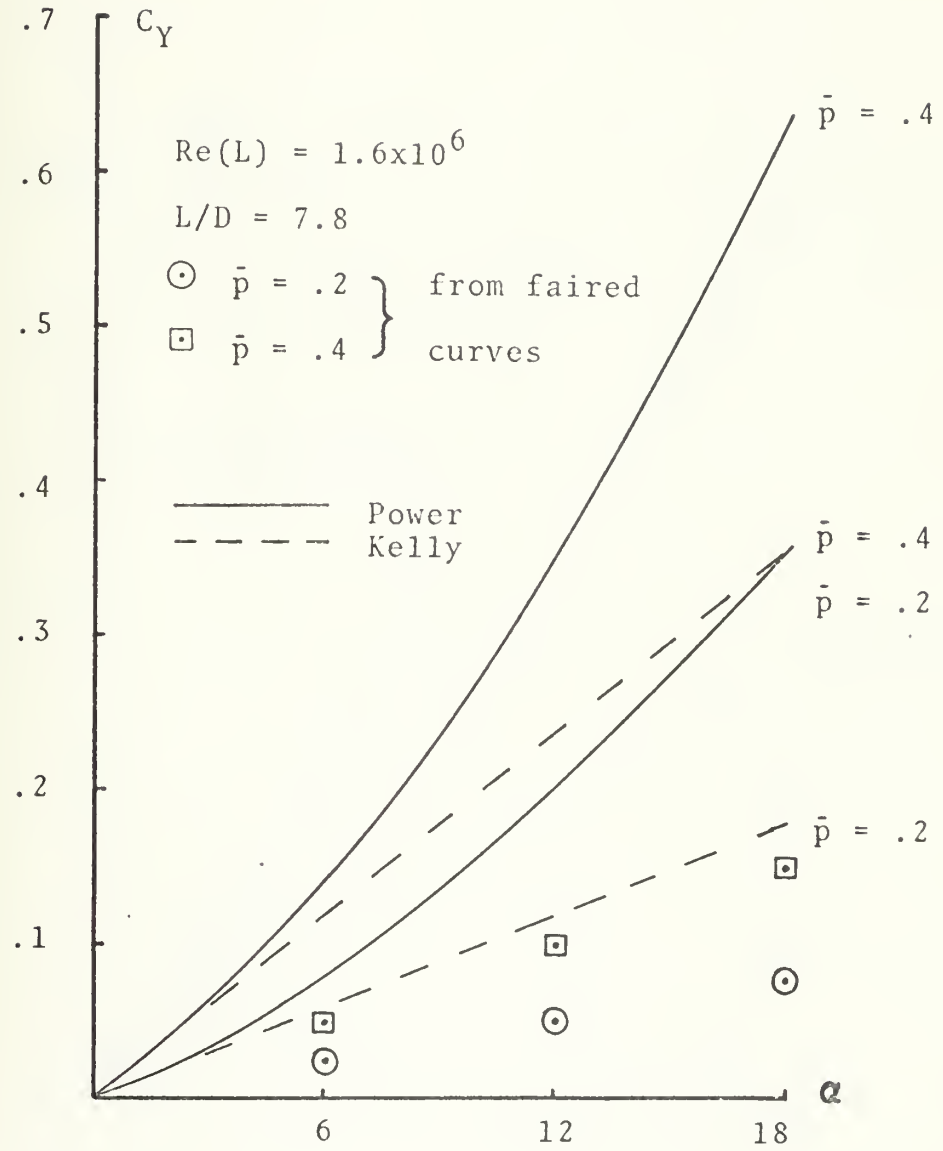

Figure 24. Magnus Force Coefficient vs. Angle of Attack

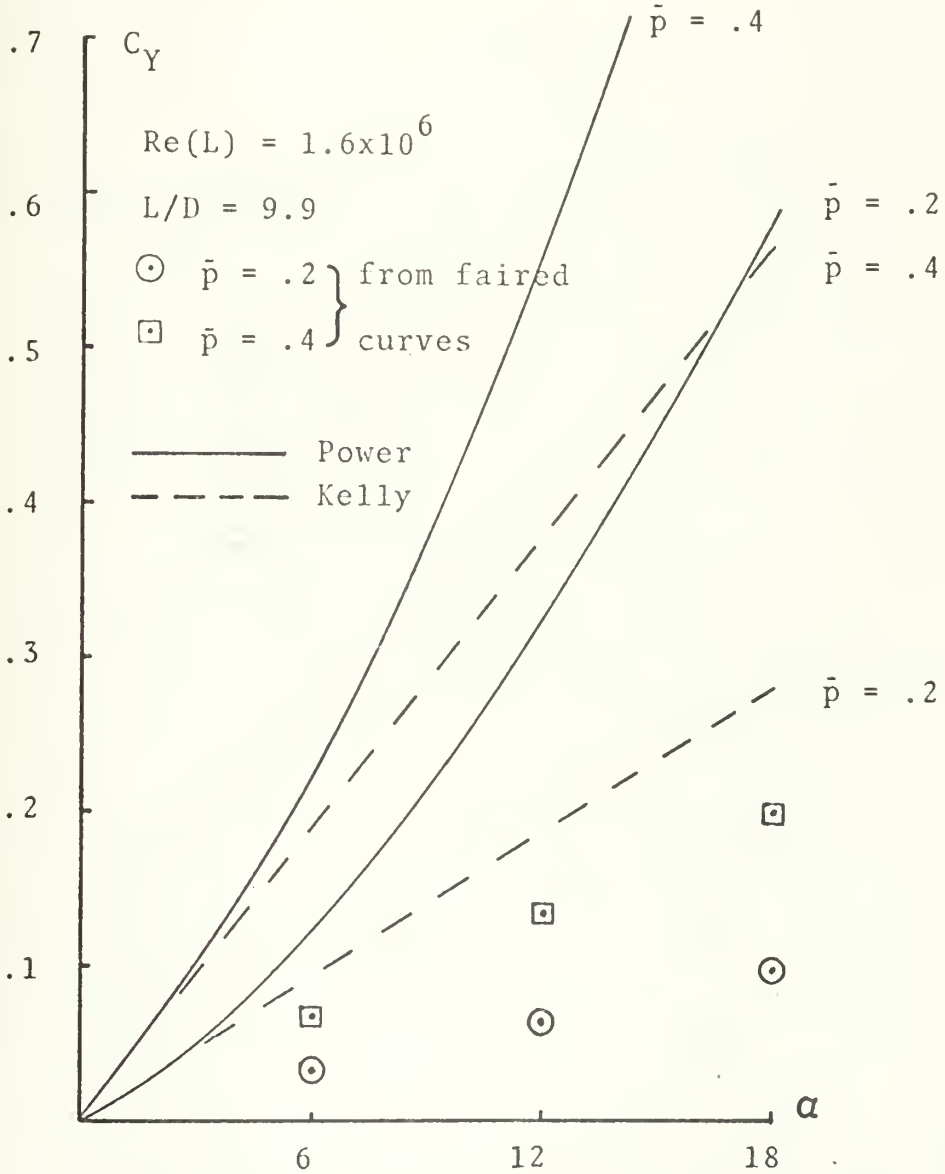

Figure 25. Magnus Force Coefficient vs. Angle of Attack

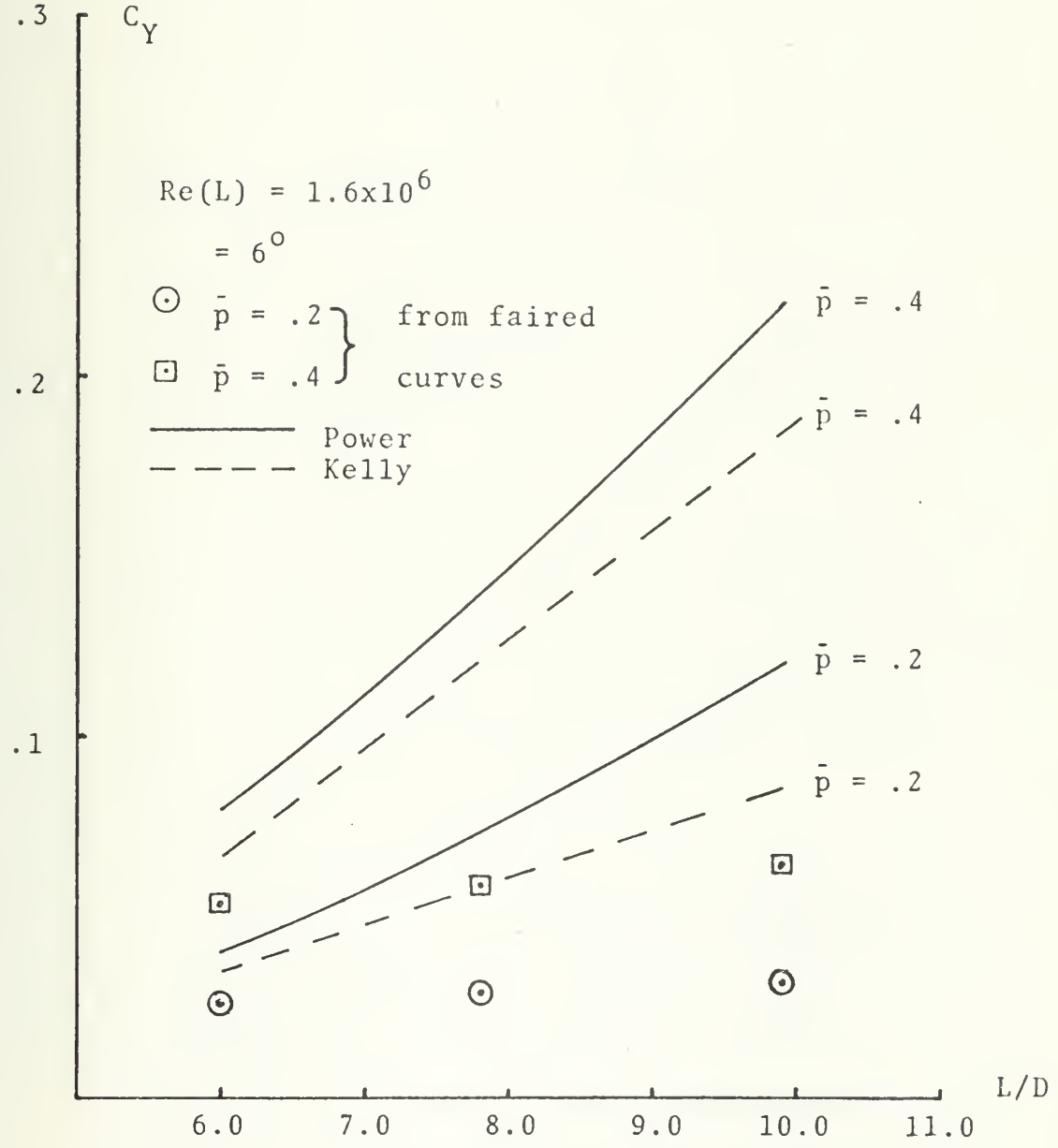

Figure 26. Magnus Force Coefficient vs. L/D

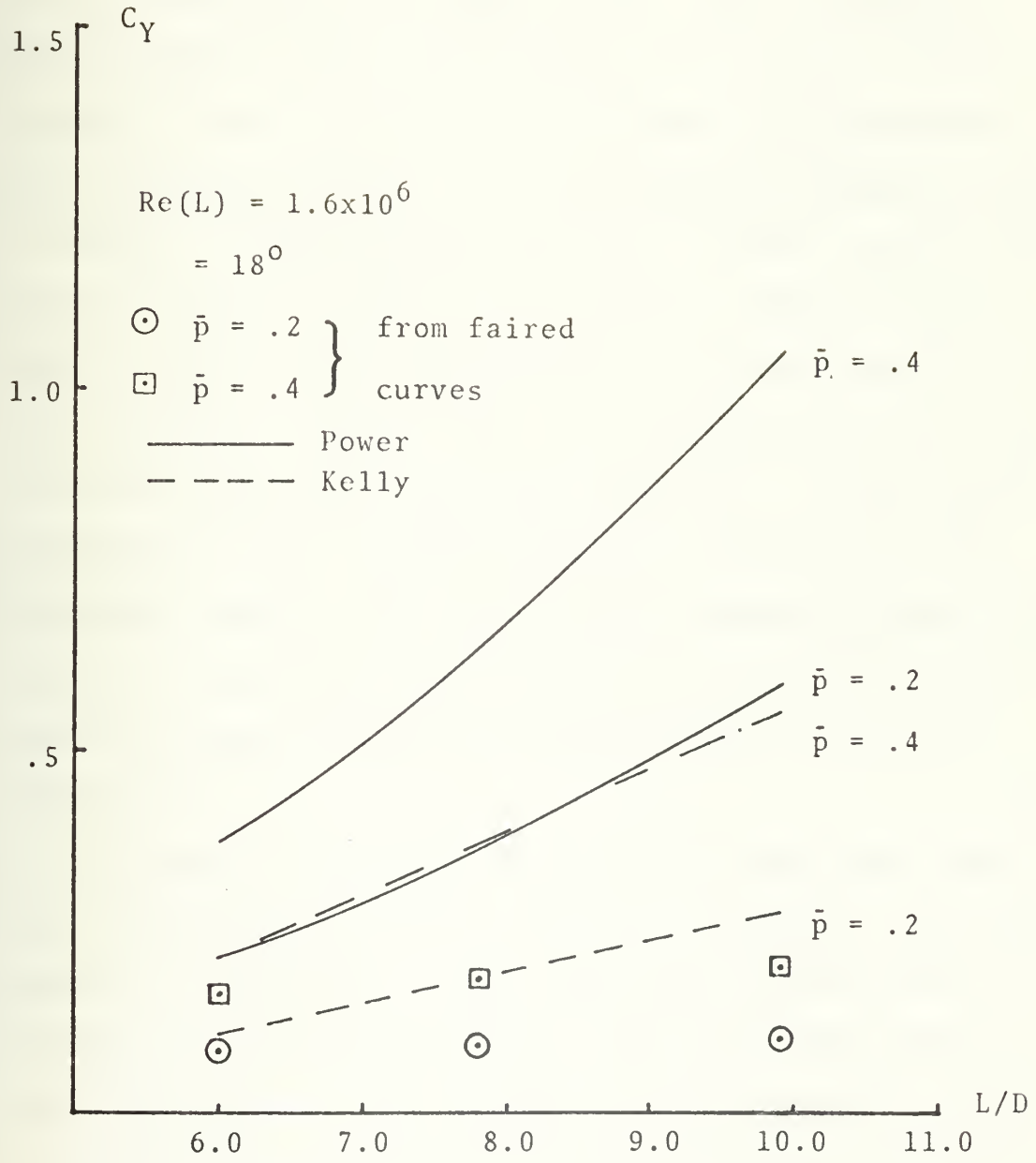

Figure 27. Magnus Force Coefficient vs. L/D

CONCLUSIONS

The graphical data suggest, but with the error bounds of the experimentation cannot verify, that the Magnus force might be linear in both α and $\bar{p}$ for small angles of attack and small spin rates at constant Reynolds numbers. Other experimenters have found non-linear variations of C_Y at angles of attack greater than 10^o. Power's theory predicts a linear variation with $\bar{p}$ and non-linear variation with α while Kelly's [7] predicts a linear variation with both $\bar{p}$ and α. However, due to the magnitude of the error associated with each data point obtained, a great deal of latitude for data interpretation was available once the data were reduced. The data scatter indicates that if the sources of error discussed in the data analysis section could be reduced, the results would be more valid for comparison.

In general the forces obtained were much lower than those predicted by Kelly's or Power's theory as shown by Figures 21 through 25. These theories were developed assuming an open-ended cylinder while the model had an ogive nose shape. This difference alone, however, cannot account for the discrepancies between theory and experimental results. Figures 26 and 27 indicate that as the length-to-diameter ratio of the missile increases, so does

the side force. However, comparison of the experimental data with theory shows that the variation of C_Y with L/D in the region of these experiments is smaller than predicted by theory.

The experimental data presented in Figures 21 through 25 were used to calculate C_1 in equation (1). The results showed C_1 to be a small negative number. This implies that flow circulation contributed negatively to the Magnus force, which contradicts physical reasoning. If $C_1=0$, the resulting equation is essentially what Kelly predicted. However, the theory must not be discounted simply because the experimental data do not support it. When the error associated with the data is considered it is readily apparent that the data may not correlate with theory.

Because the measurement of these forces is so critical, a better method for measuring them must be devised. Although the method used did provide some meaningful data which supported theory to some extent, the necessity for finer instrumentation and refinement of equipment is obvious. Precise machining was necessary for all of the apparatus, but no amount of machining or expensive, elaborate electronic equipment will enable accurate data to be obtained if other parameters such as poor tunnel flow characteristics are a part of the system. The model, as constructed, can be tested with a variety of nose shapes so that comparisons can be made of the effects different forebody shapes have on the production of Magnus forces.

However, until more accurate results are obtainable it would be useless to test different forebody shapes. Because the data obtained do indicate that some side force was measured there is sufficient reason for continuing the experimentation with re-designed equipment to obtain more meaningful results.

RECOMMENDATIONS FOR FURTHER STUDY

1. Design a more sensitive balance that is less affected by air motor hose pressurization.

2. Redesign the sting mounting so that it is isolated from test section vibrations.

3. Install flow straightening screens to reduce tunnel test section flow fluctuations.

4. Re-examine the circulation coefficient C_1 to correlate theory by taking new data with improved experimental system.

5. Perform nose shape studies to assess the affects of forebody shape on Magnus force.

TESTING DATE: 13 JANUARY 1973

MISSILE LENGTH = 17.714 INCHES (L/D = 6.0)

AOA	RE(L)	V	RPM	P-HAT	Y	CY	CY(-)	CY(+)	CY(V+)	CYPOW
0.0	7.34915E 05	86.0	0.	0.0	0.02	0.06	-0.19	0.31	0.06	0.0
0.0	7.34915E 05	86.0	-1705.	-0.26	-.01	-0.03	-0.28	0.22	-0.02	0.0
0.0	7.34915E 05	86.0	-2305.	-0.34	0.01	0.02	-0.23	0.27	0.02	0.0
0.0	7.34915E 05	86.0	-2685.	-0.40	-.04	-0.10	-0.35	0.15	-0.09	0.0
0.0	7.34915E 05	86.0	1705.	0.26	-.03	-0.06	-0.32	0.19	-0.06	0.0
0.0	7.34915E 05	86.0	2125.	0.32	0.01	0.02	-0.23	0.28	0.02	0.0
0.0	7.34915E 05	86.0	2395.	0.36	-.05	-0.12	-0.37	0.13	-0.11	0.0
0.0	7.34915E 05	86.0	2660.	0.40	-.07	-0.19	-0.44	0.06	-0.17	0.0
6.0	7.31907E 05	86.2	0.	0.0	0.10	0.25	0.00	0.50	0.22	0.0
6.0	7.31907E 05	86.2	1745.	0.26	0.07	0.18	-0.07	0.43	0.16	0.10
6.0	7.31907E 05	86.2	2160.	0.32	0.08	0.21	-0.04	0.46	0.18	0.12
6.0	7.31907E 05	86.2	2405.	0.36	0.10	0.26	0.01	0.52	0.23	0.13
6.0	7.31907E 05	86.2	2625.	0.39	0.05	0.12	-0.13	0.37	0.10	0.14
6.0	7.31907E 05	86.2	-1505.	-0.22	0.06	0.16	-0.09	0.41	0.14	-0.02
6.0	7.31907E 05	86.2	-2000.	-0.30	0.08	0.19	-0.06	0.44	0.17	-0.04
6.0	7.31907E 05	86.2	-2440.	-0.36	0.05	0.12	-0.13	0.37	0.11	-0.05
12.0	7.03677E 05	84.2	0.	0.0	0.02	0.06	-0.21	0.32	0.05	0.0
12.0	7.03677E 05	84.2	-1610.	-0.25	-.00	-0.00	-0.26	0.26	-0.00	0.04
12.0	7.03677E 05	84.2	-2145.	-0.33	-.00	-0.01	-0.27	0.26	-0.00	0.03
12.0	7.03677E 05	84.2	-2660.	-0.41	0.01	0.01	-0.25	0.28	0.01	0.01
12.0	7.03677E 05	84.2	1540.	0.24	-.01	-0.03	-0.30	0.23	-0.03	0.29
12.0	7.03677E 05	84.2	1800.	0.28	-.02	-0.05	-0.31	0.22	-0.04	0.33
12.0	7.03677E 05	84.2	2055.	0.31	0.00	0.00	-0.26	0.27	0.00	0.36
12.0	7.03677E 05	84.2	2200.	0.34	-.02	-0.06	-0.32	0.21	-0.05	0.38
18.0	6.65025E 05	81.9	0.	0.0	0.07	0.19	-0.09	0.47	0.17	0.0
18.0	6.65025E 05	81.9	-1595.	-0.25	0.04	0.11	-0.17	0.39	0.09	0.22
18.0	6.65025E 05	81.9	-1910.	-0.30	0.04	0.12	-0.16	0.40	0.10	0.24
18.0	6.65025E 05	81.9	-2060.	-0.32	0.02	0.05	-0.23	0.33	0.04	0.24
18.0	6.65025E 05	81.9	1475.	0.23	0.04	0.12	-0.16	0.40	0.10	0.59
18.0	6.65025E 05	81.9	1740.	0.27	0.01	0.02	-0.26	0.30	0.02	0.67
18.0	6.65025E 05	81.9	1915.	0.30	-.06	-0.17	-0.44	0.11	-0.14	0.72
18.0	6.65025E 05	81.9	2035.	0.32	-.16	-0.46	-0.74	-0.18	-0.40	0.76

TESTING DATE: 13 JANUARY 1973

MISSILE LENGTH = 17.714 INCHES (L/D = 6.0)

ACA	RE(L)	V	RPM	P-HAT	Y	CY	CY(-)	CY(+)	CY(V+)	CYPOW
0.0	1.67999E 06	196.7	0.	0.0	-.06	-0.03	-0.08	0.02	-0.03	0.0
0.0	1.67999E 06	196.7	-1700.	-0.11	0.02	0.01	-0.04	0.06	0.01	0.0
0.0	1.67999E 06	196.7	-2270.	-0.15	0.04	0.02	-0.03	0.07	0.02	0.0
0.0	1.67999E 06	196.7	-2620.	-0.17	0.07	0.03	-0.01	0.08	0.03	0.0
0.0	1.67999E 06	196.7	1780.	0.12	-.02	-0.01	-0.06	0.04	-0.01	0.0
0.0	1.67999E 06	196.7	2180.	0.14	0.00	0.00	-0.05	0.05	0.00	0.0
0.0	1.67999E 06	196.7	2480.	0.16	-.04	-0.02	-0.07	0.03	-0.02	0.0
0.0	1.67999E 06	196.7	2735.	0.18	-.07	-0.03	-0.08	0.02	-0.03	0.0
6.0	1.67301E 06	196.9	0.	0.0	0.07	0.03	-0.02	0.08	0.03	0.0
6.0	1.67301E 06	196.9	1620.	0.11	0.08	0.04	-0.01	0.09	0.04	0.04
6.0	1.67301E 06	196.9	2055.	0.13	0.04	0.02	-0.03	0.07	0.02	0.04
6.0	1.67301E 06	196.9	2340.	0.15	0.08	0.04	-0.01	0.09	0.04	0.05
6.0	1.67301E 06	196.9	2545.	0.17	0.05	0.02	-0.02	0.07	0.02	0.05
6.0	1.67301E 06	196.9	-1525.	-0.10	0.07	0.04	-0.01	0.08	0.03	0.00
6.0	1.67301E 06	196.9	-2400.	-0.16	0.04	0.02	-0.03	0.07	0.02	-0.00
6.0	1.67301E 06	196.9	-2600.	-0.17	0.08	0.04	-0.01	0.09	0.04	-0.01
12.0	1.68009E 06	201.1	0.	0.0	-.04	-0.02	-0.06	0.03	-0.02	0.0
12.0	1.68009E 06	201.1	-1540.	-0.10	0.04	0.02	-0.03	0.06	0.02	0.04
12.0	1.68009E 06	201.1	-2020.	-0.13	-.03	-0.01	-0.06	0.03	-0.01	0.04
12.0	1.68009E 06	201.1	-2365.	-0.15	-.02	-0.01	-0.05	0.04	-0.01	0.05
12.0	1.68009E 06	201.1	-2505.	-0.16	0.05	0.02	-0.02	0.07	0.02	0.05
12.0	1.68009E 06	201.1	2020.	0.13	-.07	-0.03	-0.08	0.02	-0.03	0.13
12.0	1.68009E 06	201.1	2150.	0.14	-.00	-0.00	-0.05	0.05	-0.00	0.14
12.0	1.68009E 06	201.1	2315.	0.15	-.07	-0.03	-0.08	0.02	-0.03	0.15
18.0	1.67997E 06	206.8	0.	0.0	-.07	-0.03	-0.07	0.01	-0.03	0.0
18.0	1.67997E 06	206.8	-1480.	-0.09	-.06	-0.02	-0.07	0.02	-0.02	0.10
18.0	1.67997E 06	206.8	-1725.	-0.11	-.02	-0.01	-0.05	0.03	-0.01	0.11
18.0	1.67997E 06	206.8	-1940.	-0.12	-.01	-0.00	-0.05	0.04	-0.00	0.12
18.0	1.67997E 06	206.8	1590.	0.10	-.01	-0.00	-0.05	0.04	-0.00	0.21
18.0	1.67997E 06	206.8	1925.	0.12	-.00	-0.00	-0.05	0.04	-0.00	0.25
18.0	1.67997E 06	206.8	2100.	0.13	-.05	-0.02	-0.07	0.02	-0.02	0.27
18.0	1.67997E 06	206.8	2180.	0.14	-.23	-0.10	-0.14	-0.06	-0.10	0.27

TESTING DATE: 17 JANUARY 1973

MISSILE LENGTH = 23.123 INCHES (L/D = 7.8)

AOA	RE(L)	V	RPM	P-HAT	Y	CY	CY(-)	CY(+)	CY(V+)	CYPOW
0.0	7.05104E 05	63.3	0.	0.0	0.02	0.09	-0.37	0.56	0.07	0.0
0.0	7.05104E 05	63.3	-1055.	-0.43	0.04	0.21	-0.26	0.67	0.17	0.0
0.0	7.05104E 05	63.3	-1115.	-0.45	-.00	-0.01	-0.47	0.46	-0.01	0.0
0.0	7.05104E 05	63.3	-1230.	-0.50	0.09	0.41	-0.06	0.87	0.32	0.0
0.0	7.05104E 05	63.3	-1235.	-0.50	0.08	0.37	-0.10	0.83	0.29	0.0
0.0	7.05104E 05	63.3	960.	0.39	0.11	0.51	0.04	0.97	0.40	0.0
0.0	7.05104E 05	63.3	1020.	0.41	0.14	0.65	0.18	1.12	0.52	0.0
0.0	7.05104E 05	63.3	1060.	0.43	0.15	0.68	0.22	1.15	0.54	0.0
6.0	7.04847E 05	63.7	0.	0.0	0.03	0.12	-0.34	0.58	0.10	0.0
6.0	7.04847E 05	63.7	1020.	0.41	0.07	0.33	-0.13	0.79	0.26	0.26
6.0	7.04847E 05	63.7	1080.	0.44	0.10	0.48	0.02	0.94	0.38	0.27
6.0	7.04847E 05	63.7	1110.	0.45	0.06	0.30	-0.16	0.76	0.24	0.27
6.0	7.04847E 05	63.7	1160.	0.47	0.10	0.48	0.02	0.94	0.38	0.28
6.0	7.04847E 05	63.7	-945.	-0.38	0.04	0.18	-0.29	0.64	0.14	-0.10
6.0	7.04847E 05	63.7	-1025.	-0.41	0.06	0.26	-0.20	0.72	0.21	-0.11
6.0	7.04847E 05	63.7	-1080.	-0.44	0.06	0.27	-0.19	0.73	0.21	-0.12
12.0	7.05513E 05	64.8	0.	0.0	0.04	0.19	-0.25	0.64	0.15	0.0
12.0	7.05513E 05	64.8	-900.	-0.36	0.04	0.20	-0.25	0.64	0.16	0.06
12.0	7.05513E 05	64.8	-995.	-0.40	0.10	0.44	-0.00	0.89	0.36	0.05
12.0	7.05513E 05	64.8	-1020.	-0.41	0.11	0.48	0.03	0.92	0.38	0.05
12.0	7.05513E 05	64.8	870.	0.35	0.11	0.48	0.03	0.92	0.38	0.68
12.0	7.05513E 05	64.8	980.	0.39	0.15	0.66	0.22	1.11	0.53	0.74
12.0	7.05513E 05	64.8	1030.	0.41	0.17	0.76	0.31	1.21	0.61	0.77
12.0	7.05513E 05	64.8	1110.	0.44	0.15	0.65	0.21	1.10	0.52	0.81
18.0	7.04313E 05	66.5	0.	0.0	0.05	0.21	-0.22	0.63	0.17	0.0
18.0	7.04313E 05	66.5	900.	0.35	0.08	0.36	-0.07	0.78	0.29	1.40
18.0	7.04313E 05	66.5	930.	0.36	0.10	0.42	-0.00	0.84	0.34	1.44
18.0	7.04313E 05	66.5	975.	0.38	0.12	0.52	0.10	0.95	0.43	1.48
18.0	7.04313E 05	66.5	1020.	0.39	0.09	0.38	-0.04	0.81	0.31	1.51
18.0	6.85973E 05	64.8	-845.	-0.34	0.03	0.15	-0.30	0.59	0.12	0.48
18.0	6.85973E 05	64.8	-890.	-0.35	0.07	0.33	-0.11	0.78	0.27	0.48
18.0	6.85973E 05	64.8	-925.	-0.37	0.06	0.27	-0.17	0.72	0.22	0.48

TESTING DATE: 17 JANUARY 1973

MISSILE LENGTH = 23.123 INCHES (L/D = 7.8)

AOA	RE(L)	V	RPM	P-HAT	Y	CY	CY(-)	CY(+)	CY(V+)	CYPOW
0.0	1.61123E 06	144.7	0.	0.0	0.12	0.10	0.02	0.19	0.10	0.0
0.0	1.61123E 06	144.7	-995.	-0.18	0.10	0.09	0.00	0.18	0.09	0.0
0.0	1.61123E 06	144.7	-1060.	-0.19	0.10	0.09	0.00	0.18	0.08	0.0
0.0	1.61123E 06	144.7	-1085.	-0.19	0.10	0.09	0.00	0.18	0.08	0.0
0.0	1.61123E 06	144.7	-1120.	-0.20	0.05	0.04	-0.05	0.13	0.04	0.0
0.0	1.61123E 06	144.7	-1200.	-0.21	0.11	0.10	0.01	0.19	0.09	0.0
0.0	1.61123E 06	144.7	1045.	0.19	0.16	0.14	0.05	0.23	0.13	0.0
0.0	1.61123E 06	144.7	1110.	0.20	0.16	0.14	0.05	0.23	0.13	0.0
6.0	1.61187E 06	145.6	0.	0.0	0.09	0.08	-0.00	0.17	0.08	0.0
6.0	1.61187E 06	145.6	925.	0.16	0.12	0.11	0.02	0.20	0.10	0.09
6.0	1.61187E 06	145.6	1000.	0.18	0.15	0.13	0.05	0.22	0.12	0.10
6.0	1.61187E 06	145.6	1160.	0.21	0.17	0.15	0.06	0.23	0.13	0.11
6.0	1.61187E 06	145.6	-935.	-0.17	0.09	0.08	-0.01	0.16	0.07	-0.01
6.0	1.61187E 06	145.6	-990.	-0.18	0.10	0.09	-0.00	0.17	0.08	-0.01
6.0	1.61187E 06	145.6	-1025.	-0.18	0.12	0.10	0.02	0.19	0.10	-0.01
6.0	1.61187E 06	145.6	-1060.	-0.19	0.11	0.10	0.01	0.19	0.09	-0.01
12.0	1.61141E 06	148.0	0.	0.0	0.07	0.06	-0.03	0.14	0.05	0.0
12.0	1.61141E 06	148.0	-860.	-0.15	0.08	0.07	-0.01	0.16	0.06	0.10
12.0	1.61141E 06	148.0	-945.	-0.16	0.11	0.09	0.01	0.18	0.09	0.10
12.0	1.61141E 06	148.0	-1000.	-0.17	0.11	0.10	0.01	0.18	0.09	0.10
12.0	1.61141E 06	148.0	-1060.	-0.18	0.13	0.11	0.03	0.20	0.10	0.11
12.0	1.61141E 06	148.0	920.	0.16	0.15	0.13	0.05	0.22	0.12	0.29
12.0	1.61141E 06	148.0	940.	0.16	0.16	0.13	0.05	0.22	0.12	0.30
12.0	1.61141E 06	148.0	1020.	0.18	0.02	0.02	-0.07	0.10	0.02	0.32
18.0	1.61199E 06	152.2	0.	0.0	0.07	0.05	-0.03	0.13	0.05	0.0
18.0	1.61199E 06	152.2	830.	0.14	0.14	0.11	0.03	0.19	0.10	0.51
18.0	1.61199E 06	152.2	925.	0.16	0.21	0.17	0.09	0.25	0.16	0.56
18.0	1.61199E 06	152.2	1020.	0.17	0.12	0.10	0.02	0.18	0.09	0.61
18.0	1.61199E 06	152.2	1080.	0.18	0.17	0.14	0.06	0.22	0.13	0.65
18.0	1.61199E 06	152.2	-840.	-0.14	0.01	0.01	-0.07	0.09	0.01	0.26
18.0	1.61199E 06	152.2	-920.	-0.16	0.02	0.01	-0.07	0.09	0.01	0.28
18.0	1.61199E 06	152.2	-925.	-0.16	0.02	0.02	-0.06	0.10	0.02	0.28

TESTING DATE: 5 FEBRUARY 1973

MISSILE LENGTH = 29.121 INCHES (L/D = 9.9)

AOA	RE(L)	V	RPM	P-HAT	Y	CY	CY(-)	CY(+)	CY(V+)	CYPOW
0.0	1.71414E 06	120.1	0.	0.0	0.13	0.17	0.05	0.30	0.16	0.0
0.0	1.71414E 06	120.1	810.	0.17	0.13	0.17	0.04	0.30	0.16	0.0
0.0	1.71414E 06	120.1	1040.	0.22	0.14	0.19	0.06	0.31	0.17	0.0
0.0	1.71414E 06	120.1	0.	0.0	0.09	0.12	-0.01	0.25	0.11	0.0
0.0	1.71414E 06	120.1	-1020.	-0.22	0.09	0.12	-0.01	0.25	0.11	0.0
0.0	1.71414E 06	120.1	-1040.	-0.22	0.12	0.15	0.02	0.28	0.14	0.0
0.0	1.71414E 06	120.1	-955.	-0.20	0.09	0.12	-0.01	0.25	0.11	0.0
0.0	1.71414E 06	120.1	-760.	-0.16	0.13	0.17	0.04	0.29	0.15	0.0
6.0	1.79289E 06	126.3	0.	0.0	0.09	0.11	-0.01	0.22	0.10	0.0
6.0	1.79289E 06	126.3	780.	0.16	0.16	0.19	0.07	0.30	0.18	0.14
6.0	1.79289E 06	126.3	860.	0.18	0.13	0.15	0.04	0.27	0.14	0.15
6.0	1.79289E 06	126.3	1015.	0.21	0.03	0.03	-0.08	0.15	0.03	0.17
6.0	1.79289E 06	126.3	1085.	0.22	-.13	-0.15	-0.26	-0.03	-0.14	0.18
6.0	1.79289E 06	126.3	-1080.	-0.22	0.27	0.31	0.19	0.42	0.29	-0.01
6.0	1.79289E 06	126.3	-990.	-0.20	0.22	0.26	0.14	0.37	0.24	-0.01
6.0	1.79289E 06	126.3	-840.	-0.17	0.13	0.15	0.04	0.27	0.14	-0.00
12.0	1.71420E 06	122.8	0.	0.0	0.16	0.20	0.08	0.32	0.19	0.0
12.0	1.71420E 06	122.8	-865.	-0.18	0.12	0.14	0.02	0.26	0.13	0.19
12.0	1.71420E 06	122.8	-1100.	-0.23	0.16	0.20	0.08	0.32	0.19	0.20
12.0	1.71420E 06	122.8	-1165.	-0.24	0.24	0.29	0.17	0.41	0.27	0.20
12.0	1.71420E 06	122.8	-1280.	-0.27	0.30	0.37	0.25	0.49	0.35	0.20
12.0	1.71420E 06	122.8	1070.	0.22	-.06	-0.07	-0.19	0.05	-0.07	0.61
12.0	1.71420E 06	122.8	945.	0.20	0.14	0.17	0.05	0.29	0.16	0.55
12.0	1.71420E 06	122.8	770.	0.16	0.18	0.22	0.10	0.34	0.21	0.47
18.0	1.71453E 06	126.3	0.	0.0	0.13	0.15	0.03	0.26	0.14	0.0
18.0	1.71453E 06	126.3	780.	0.16	0.11	0.12	0.01	0.24	0.12	0.93
18.0	1.71453E 06	126.3	1080.	0.22	0.11	0.13	0.01	0.24	0.12	1.23
18.0	1.71453E 06	126.3	1230.	0.25	-.02	-0.02	-0.14	0.10	-0.02	1.36
18.0	1.71453E 06	126.3	-1220.	-0.25	0.33	0.39	0.27	0.50	0.36	0.68
18.0	1.71453E 06	126.3	-1150.	-0.23	0.22	0.25	0.14	0.37	0.24	0.65
18.0	1.71453E 06	126.3	-1070.	-0.22	-.11	-0.13	-0.25	-0.02	-0.12	0.62
18.0	1.71453E 06	126.3	-870.	-0.18	0.05	0.06	-0.06	0.18	0.06	0.54

```
COMPUTER PROGRAM TO REDUCE RAW DATA TO DETERMINE MAGNUS
FORCE AND COEFFICIENT WITH ERROR BOUNDS

      DIMENSION ALIST(100),BLIST(100),FLIST(100),GLIST(100),
       PLIST(100),CLIST(100)

    EXPLANATION OF SYMBOLS USED IN THE PROGRAM
          XL/XLF  - MISSILE LENGTH (IN./FT.)
            DF    - MISSILE DIAMETER IN FEET
           XLD    - MISSILE LENGTH-TO-DIAMETER RATIO
          T/TR    - TEMPERATURE (FAHRENHEIT/RANKINE)
             P    - ATMOSPHERIC PRESSURE (IN. HG.)
           RHO    - ATMOSPHERIC DENSITY
           XMU    - COEFFICIENT OF VISCOSITY (AIR)
             R    - GAS CONSTANT
             G    - GRAVITY CONSTANT
        XMF/XMA   - SLOPES OF MOMENT VS CHART DEFLECTION
                    FROM STING CALIBRATION
            DF    - DIAMETER OF MISSILE (FT.)
        AOA/ARAD  - ANGLE OF ATTACK (DEGREES/RADIANS)
             Q    - DYNAMIC PRESSURE IN CM H2O
          V/VTRU  - TUNNEL VELOCITY (MEASURED/CORRECTED)
           EPS    - VELOCITY CORRECTION FACTOR
          TSEC    - TEST SECTION CROSS SECTIONAL AREA
           XCO    - LENGTH OF MISSILE NOSE SHAPE
          CONE    - VOLUME OF MISSILE NOSE PIECE
           VOL    - VOLUME OF MISSILE
        REV/XO    - REVOLUTIONS PER MINUTE/RADIANS PER
                    SECOND
        REL/REC   - REYNOLDS NUMBERS BASED ON LENGTH/CROSS
                    FLOW
           XCO    - LENGTH OF MISSILE NOSE SHAPE
             S    - MISSILE CROSS SECTIONAL AREA
       FCOR/ACOR  - CORRECTIONS TO DATA DUE TO EFFECTS OF
                    HOSE STIFFENING ON STING


      WRITE(6,10)


    READ IN CIRCULATION FUNCTION DATA FOR USE IN POWER'S
    THEORETICAL EQUATION FOR MAGNUS FORCE COEFFICIENT

      READ(5,14)(PLIST(J),J=1,17)
      READ(5,14)(CLIST(J),J=1,17)

      DO 100 I=1,10
      READ(5,11)L,NDATE,M,E
      IF(E.EQ.1.0)GO TO 9
      IF(E.GT.5.0)GO TO 1
      WRITE(6,12)NDATE
      GO TO 2
    1 WRITE(6,13)NDATE

    READ IN DATA FOR FORCE READING CORRECTIONS DUE TO HOSE
    AIR PRESSURES

    2 READ(5,14)(ALIST(J),J=1,L)
      READ(5,14)(BLIST(J),J=1,L)
      READ(5,14)(FLIST(J),J=1,L)
      READ(5,14)(GLIST(J),J=1,L)


      DO 101 N=1,M

    READ IN MISSILE LENGTH, TEMPERATURE (DEGREES
    FAHRENHEIT), ATMOSPHERIC PRESSURE, AND A MISSILE
    PARAMETER USED TO DETERMINE LOCATION OF CENTER OF
    PRESSURE

      READ(5,15)XL,T,P,D,K
       XLF = XL/12.
```

```
      DF = 2.950/12.
     XLD = XLF/DF
   WRITE(6,16)XL,XLD

      TR = T+459.67
       R = 53.34
       G = 32.174
     RHO = P*2116.22/(29.92*G*R*TR)
       X = 2.26967 E-08
     XMU = X*(TR**1.5)/(TR+198.72)
     XMF = 63.7/274.8
     XMA = 86.4/323.7


   DO 102 J=1,K

READ IN MISSILE ANGLE OF ATTACK, DYNAMIC PRESSURE IN
CM H2O (CORRECTED TO TRUE Q IN PROGRAM), THE
REVOLUTIONS PER MINUTE, AND THE TWO CHARTLINE
READINGS (1 CHARTLINE PER MILLIVOLT)

   READ(5,17)AOA,Q,REV,VF,VA,PHOSE
   SPIN = REV
   ANGL = ABS(AOA)
   ARAD = ANGL*3.14159/180.
     CA = COS(ARAD)
     SA = SIN(ARAD)
      Z = Q*62.4*1.133/(RHO*15.24)
      V = SQRT(Z)


INSERT DATA TO DETERMINE VELOCITY ERROR BOUND

   IF(Q.GT.10.00)GO TO 3
     QX = Q+0.5
   GO TO 4
3    QX = Q+1.0
4    ZP = QX*62.4*1.133/(RHO*15.24)
     VP = SQRT(ZP)

   TSEC = 14.41
   CONF =    .01973
    XCO = 7.244/12.
    VOL = CONF+3.14159*(DF**2)*(XLF-XCO)/4.
    EPS = .75*((3.14159/4.)**.5)*(1.+.4*DF/XLF)*VOL/
     (TSEC**1.5)
   VTRU = V*(1.+EPS)
   VTRP = VP*(1.+EPS)
5    XO = REV*2.*3.14159/60.
6    PB = DF*XO/VTRU
    PBP = DF*XO/VTRP
    REL = RHO*XLF*VTRU*CA/XMU
    REC = RHO*DF*VTRU*SA/XMU
      S = ((DF/2.)**2)*3.14159

   FCOR = PIF2(PHOSE,ALIST,L,BLIST)
    VFC = VF-FCOR
   ACOR = PIF2(PHOSE,FLIST,L,GLIST)
    VAC = VA-ACOR
   XMOF = XMF*VFC
   XMOA = XMA*VAC


DATA INPUT FOR DETERMINING ERROR IN INITIAL RAW DATA
READINGS

     VFP = VFC+1.0
     VFM = VFC-1.0
     VAP = VAC+1.0
     VAM = VAC-1.0
    XMFP = XMF*VFP
    XMFM = XMF*VFM
```

```
      XMAP = XMA*VAP
      XMAM = XMA*VAM

C     CALCULATION OF MAGNUS FORCE, FORCE COEFFICIENT, AND
C     ERROR BOUND

         Y = (XMOA-XMOF)/5.
       XCP = XMOF/Y
        CY = 2.*Y/(RHO*VTRU*VTRU*S)
        YP = (XMAM-XMFP)/5.
       CYP = 2.*YP/(RHO*VTRU*VTRU*S)
        YM = (XMAP-XMFM)/5.
       CYM = 2.*YM/(RHO*VTRU*VTRU*S)
      CYVP = 2.*Y/(RHO*VTRP*VTRP*S)

      IF(AOA.LT.1.0)GO TO 7
      IF(PB.EQ.0.0)GO TO 7
      PSIN = ABS(PB/SA)
         F = PIF2(PSIN,PLIST,17,CLIST)
        C1 = .6*ARAD*F/(128.*3.14159*PB)
      CYPW = (ARAD*PB*XLD*XLD/(REL**.5))*(60.97+(256.*C1*
     (REC**.75)-357.37)*XLD/(REL**.5)-227.01*XLD*XLD/REL)
      GO TO 8
    7 CYPW = 0.0

C     PRINTOUT DATA DESIRED

    8 WRITE(6,18)AOA,REL,VTRU,SPIN,PB,Y,CY,CYP,CYM,CYVP,CYPW

  102 CONTINUE
  101 CONTINUE
  100 CONTINUE

C     FORMAT CONTROL STATEMENTS ARE:

   10 FORMAT(///T40,'APPENDIX B'///T31,'MAGNUS FORCE AND',
     1X,'COEFFICIENT')
   11 FORMAT(3I5,F5.1)
   12 FORMAT(////4X,'TESTING DATE:',I3,1X,'JANUARY 1973')
   13 FORMAT(////4X,'TESTING DATE:',I3,1X,'FEBRUARY 1973')
   14 FORMAT(7F10.1)
   15 FORMAT(F10.3,F10.1,2F10.2,I5)
   16 FORMAT(//5X,'MISSILE LENGTH = ',F6.3,1X,'INCHES',1X,
     '(L/D = ',F3.1,')'//6X,'AOA',6X,'RE(L)',7X,'V',5X,
     'RPM',3X,'P-HAT',3X,'Y',5X,'CY',3X,'CY(-)',2X,'CY(+)'
     .2X,'CY(V+)',1X,'CYPOW')
   17 FORMAT(F10.1,F10.2,4F10.1)
   18 FORMAT('0',4X,F4.1,1X,1PE12.5,2X,0PF5.1,2X,F6.0,2X,
     F4.1,2X,F4.2,7(2X,F5.2))
   19 FORMAT(7F10.3)

    9 STOP
      END



      FUNCTION PIF2(X,FLIST,N,GLIST)
      SUBPROGRAM FUNCTION 2ND ORDER LOOKUP
      DIMENSION FLIST(100),GLIST(100)
      BLIF(P,Q,R,S,T)=((Q-P)*(S-T)/(R-Q)+S)
      IF (X-FLIST(N)) 2,1,1
    1 I=N-1
      GO TO 5
    2 IF(X-FLIST(1)) 4,4,6
    4 I=1
    5 K=1
      GO TO 30
    6 K=2
```

```
 7 DO 8  I=1,N
   IF (X-FLIST(I)) 9,9,8
 8 CONTINUE
   I=N
 9 I=I-1
30 BLIF1=BLIF(X,FLIST(I),FLIST(I+1),GLIST(I),GLIST(I+1))
10 IF (K-1)  11,11,12
11 PIF2 = BLIF1
   RETURN
12 IF((I+2)-N)  13,13,16
13 IF((I-1)-1)  15,14,14
14 IF (ABS (FLIST(I-1)-X) -ABS (FLIST(I+2)-X))  16,15,15
15 L=I+2
   GO TO 17
16 L=I-1
17 BLIF2=BLIF(X,FLIST(I),FLIST(L),GLIST(I),GLIST(L))
   PIF2=BLIF(X,FLIST(I+1),FLIST(L),BLIF1,BLIF2)
18 RETURN
   END
```

LIST OF REFERENCES

1. Swanson, W. M., "The Magnus Effect: A Summary of Investigations to Date," Journal of Basic Engineering, pp. 461-470, September 1961.

2. Magnus, G., "Uber die Aberwucheing der Geschosie," Abhandle d. Klg, Akad d. Wiss zer Berlin, Poggendorffs Annelen der Physiks 88, I, 1853.

3. Lord Rayleigh, "On the Irregular Flight of a Tennis Ball," Messenger of Mathematics, v. 7, p. 14, 1877.

4. Flettner, Anton, "The Flettner Rotor Ship," Engineering, v. 19, pp. 117-120, 23 January 1925.

5. Prandtl, L., Application of the Magnus Effect to the Wind Propulsion of Ships, National Advisory Committee for Aeronautics (NACA TM 367), 1924.

6. Martin, J. C., On Magnus Effects Caused by the Boundary-Layer Displacement Thickness on Bodies of Revolution at Small Angles of Attack, Ballistic Research Laboratory (BRL Report 870), June 1953.

7. Kelly, H. R., An Analytical Method for Predicting the Magnus Forces and Moments on Spinning Projectiles, Atomic Energy Commission (AEC Report TM-1634), 12 August 1954.

8. Power, H. L., Boundary Layer Contribution to the Magnus Effect on a Spinning Cylinder at Low Angles of Attack, Ph.D. Thesis, Iowa State University, Iowa City, 1971.

9. Pankhurst, R. C. and Holder, D. W., Wind-Tunnel Technique, Sir Isaac Pitman & Sons Ltd., 1968.

10. Fletcher, C. A. J., Investigation of the Magnus Characteristics of a Spinning Inclined Ogive-Cylinder Body at M = .2, Australian Defense Scientific Service (Technical Note WRE-TN-HSA-159), October 1969.

11. Gorlin, S. M. and Slezinger, I. I., Wind Tunnels and Their Instrumentation, Israel Program of Scientific Translations, 1966.

12. Griffiths, R. T. and Ma, C. Y., "Differential Boundary-Layer Separation Effects in the Flow over a Rotating Cylinder," The Aeronautical Journal of the Royal Aeronautical Society, v. 73, pp. 524-526, June 1969.

13. Hauer, H. J., and Kelly, H. R., The Subsonic Aerodynamic Characteristics of Spinning Cone-Cylinders and Ogive-Cylinders at Large Angles of Attack, U.S. Naval Ordnance Test Station (NAVORD Report 3529), 11 July 1955.

14. Houghton, E. L., and Brock, A. E., Aerodynamics for Engineering Students, St. Martin's Press, 1970.

15. Kelly, H. R. and Thacker, G. R., The Effect of High Spin on the Magnus Force on a Cylinder at Small Angles of Attack, U.S. Naval Ordnance Test Station (NAVORD Report 5036), 29 February 1956.

16. Luchuk, W. and Sparks, W., Wind Tunnel Magnus Characteristics of the 7-Caliber Army-Navy Spinner Rocket, U.S. Naval Ordnance Laboratory (NAVORD Report 3813), 10 September 1954.

17. Platou, A. S., "Magnus Characteristics of Finned and Non-Finned Projectiles," AIAA Journal, v. 3, no. 1, pp. 83-90, January 1965.

18. Platou, A. S. and Ricci, H. A., Wind Tunnel Tests of Solid State Strain Gages, Ballistic Research Laboratory (BRL Memorandum 1928), July 1968.

19. Platou, A. S., Colburn, R., and Pedgonay, J. S., The Design and Dynamic Balancing of Spinning Models an a Testing Technique for Obtaining Magnus Data in Wind Tunnels, Ballistic Research Laboratory (BRL Memorandum 2019), October 1969.

20. Pope, Alan, Wind Tunnel Testing, 2nd ed., John Wiley & Sons, 1954.

21. Shames, Irving H., Mechanics of Fluids, McGraw Hill Book Company, 1962.

INITIAL DISTRIBUTION LIST

		No. Copies
1.	Defense Documentation Center Cameron Station Alexandria, Virginia 22314	2
2.	Library, Code 0212 Naval Postgraduate School Monterey, California 93940	2
3.	Professor R. W. Bell, Code 57Be Department of Aeronautics Naval Postgraduate School Monterey, California 93940	1
4.	Asst. Professor H. L. Power, Code 57Ph Department of Aeronautics Naval Postgraduate School Monterey, California 93940	2
5.	LT Timothy R. Beard, USN 945 Dickson Parkway Mansfield, Ohio 44907	2

DOCUMENT CONTROL DATA - R & D

(Security classification of title, body of abstract and indexing annotation must be entered when the overall report is classified)

ORIGINATING ACTIVITY (Corporate author)

Naval Postgraduate School
Monterey, California 93940

2a. REPORT SECURITY CLASSIFICATION
UNCLASSIFIED

2b. GROUP

REPORT TITLE

AN INVESTIGATION OF THE PRODUCTION OF MAGNUS FORCES ON A HIGH FINENESS RATIO BODY OF REVOLUTION

DESCRIPTIVE NOTES (Type of report and inclusive dates)
Master's Thesis; March 1973

AUTHOR(S) (First name, middle initial, last name)

REPORT DATE	7a. TOTAL NO. OF PAGES	7b. NO. OF REFS
	69	21

CONTRACT OR GRANT NO.

PROJECT NO.

9a. ORIGINATOR'S REPORT NUMBER(S)

9b. OTHER REPORT NO(S) (Any other numbers that may be assigned this report)

DISTRIBUTION STATEMENT

Approved for public release; distribution unlimited.

SUPPLEMENTARY NOTES

12. SPONSORING MILITARY ACTIVITY
Naval Postgraduate School
Monterey, California 93940

ABSTRACT

A high fineness ratio body of revolution with an ogive forebody shape was tested at varying angles of attack, Reynolds numbers, and spin rates to measure the Magnus forces developed. The experimental data were compared with previously derived theoretical equations for an open-ended cylinder of revolution to substantiate the theoretical work.

KEY WORDS	LINK A		LINK B		LINK C	
	ROLE	WT	ROLE	WT	ROLE	WT
Magnus						
Spin						
Rotate						

Thesis
B295
c.1

142007

Beard

An investigation of the production of Magnus forces on a high fineness ratio body of revolution.